41p.

NASA TN D-1426

N62-16011

TECHNICAL NOTE

D-1426

COMPARISON OF EXPERIMENTAL AND NUMERICAL RESULTS FOR THE FLOW OF A PERFECT GAS ABOUT BLUNT-NOSED BODIES

By Mamoru Inouye and Harvard Lomax

Ames Research Center
Moffett Field, Calif.

NATIONAL AERONAUTICS AND SPACE ADMINISTRATION

WASHINGTON

September 1962

NATIONAL AERONAUTICS AND SPACE ADMINISTRATION

TECHNICAL NOTE D-1426

COMPARISON OF EXPERIMENTAL AND NUMERICAL RESULTS FOR THE FLOW OF A PERFECT GAS ABOUT BLUNT-NOSED BODIES

By Mamoru Inouye and Harvard Lomax

SUMMARY

The inviscid flow of a perfect gas over blunt-nosed axisymmetric and two-dimensional bodies at zero angle of attack has been calculated numerically on an IBM 7090 computer. The computation consisted of the Fuller blunt-body solution for the subsonic and transonic regions and the method of characteristics for the supersonic region. The flow fields about a number of blunt bodies were studied, and the calculated results showed good agreement with experimental shock-wave shapes, surface-pressure distributions, and flow-field surveys.

INTRODUCTION

Knowledge of the inviscid flow about blunt-nosed bodies traveling at supersonic velocities is necessary for predicting their aerodynamic and heat-transfer characteristics. Several numerical methods for calculating these flow fields have been developed and are to be found in the literature; see, for example, references 1 through 5. These methods are generally similar in that each uses a special technique for calculating the flow in the subsonic region and for providing initial data to begin a method of characteristics solution for the remainder of the flow field. One such method solves the subsonic flow problem by starting with a given shock-wave shape and "marching forward" toward the body. The purpose of the present report is to compare the results of this particular method for a perfect gas with a number of experimental results and to show that computations of this type are valid over a wide range of free-stream conditions and body shapes.

SYMBOLS

A	shock-wave shape parameter (see eq. (1))
B_s	shock bluntness (see eq. (1))
d	body diameter
l	body length
M	Mach number
p	pressure
p_i	impact pressure
r,x	cylindrical coordinates with origin at stagnation point on body
Re_∞	Reynolds number, $\frac{V_\infty d}{\nu_\infty}$
R_s	radius of curvature of the shock wave at the plane or axis of symmetry
T	temperature
V	velocity
x,y	Cartesian coordinates with origin at stagnation point on body
γ	ratio of specific heats
Δ	shock standoff distance
θ	stream angle
μ	Mach angle
ν	kinematic viscosity
ρ	density
φ	angle subtended by circular arc measured from stagnation point

Subscripts

st stagnation point

∞ free stream

DESCRIPTION OF CALCULATION METHOD

Solution in the Nose Region

The Fuller blunt-body solution (ref. 6) is used to obtain the flow field in the subsonic and transonic regions. This solution is a modification of Van Dyke's earlier work reported in references 7 and 8. The modifications include the addition of a smoothing procedure in the calculations, the use of two parameters to describe the shock-wave shape, and a nonorthogonal sheared coordinate system as shown in the sketch. Use of these modifications results in solutions of the flow field for a broader range of body shapes. Although results for only two-dimensional bodies are discussed in reference 6, the method has been programmed for an IBM 704 or 7090 computer for axisymmetric bodies as well. The solution is at present restricted to a perfect gas with a constant ratio of specific heats.

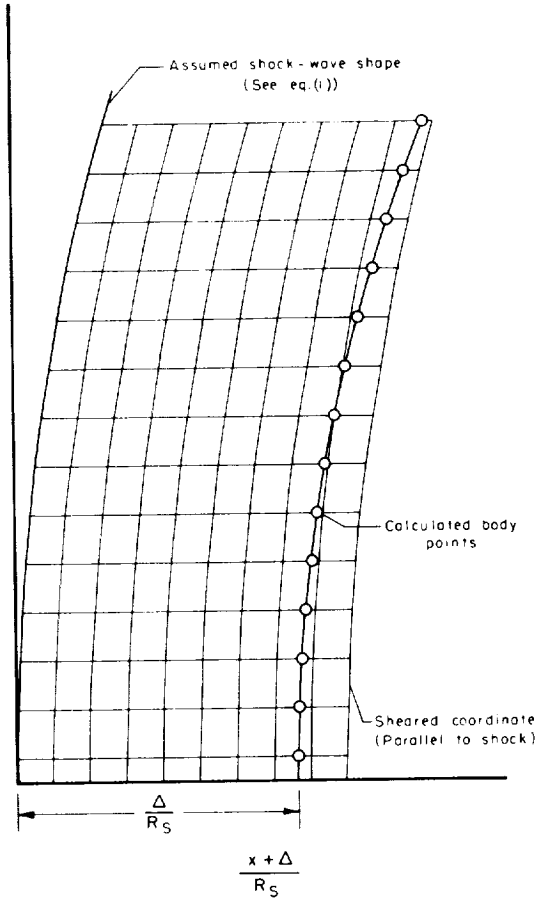

The solutions found by both Van Dyke and Fuller are commenced with the assumption of a shock shape and free-stream values of Mach number and γ. In Fuller's case the shock shape is given by the following equation ($r = y$ for two-dimensional case),

$$\frac{x + \Delta}{R_S} = \left(1 + \frac{Ar^2}{R_S{}^2}\right) \frac{1 - \sqrt{1 - (B_S r^2/R_S{}^2)}}{B_S} \qquad (1)$$

where B_S is a measure of shock-wave bluntness ($B_S = 1$, $A = 0$ corresponds to a sphere) and A is a measure of the variance from a conic section.

The equations of motion are integrated numerically, beginning at the shock wave and proceeding toward the body until sufficient flow field and body points have been calculated. If the calculated and actual body shapes are not reasonably close, this procedure is repeated with another shock shape. For a hemispherical nose, a solution can be obtained in two or three attempts if the shock-wave shape is assumed to be a conic section (A = 0). The summary of solutions in reference 8 is helpful in this regard. The parameter, A, can be used to refine these solutions or to obtain other body shapes.

Input Conditions to Start the Method of Characteristics

Because of the instabilities in the solution for the nose region, it is abandoned in favor of the method of characteristics when the flow becomes supersonic. The input conditions for the method of characteristics must, of course, lie entirely in the supersonic region. In fact, they must lie downstream of the limiting characteristic line, the line along which a disturbance cannot affect the subsonic portion of the flow field. In this report, the input conditions were selected so that the lowest local Mach number was greater than 1.03, and the locus of starting points formed a line approximately normal to the streamlines. This procedure caused no difficulty, except in the vicinity of the body,[1] and the difficulty there was overcome, for practical purposes, by extrapolation of the flow properties away from the body into the body itself. Additional points in the field were obtained by interpolation between points calculated in the blunt-body solution. Unfortunately such a procedure requires some individual attention for each case, and a general program connecting the subsonic and supersonic regions has not yet been produced. However, replacing the "marching forward" technique, described previously, by the characteristic approach, changed the method from one inherently unstable to one inherently stable. Therefore, the errors brought about by the required extrapolations and interpolations can be expected to damp out. The fact that these errors were small and, at least, did not grow is verified by subsequent calculations and comparisons with experiment.

Method of Characteristics Solution in the Supersonic Region

The method of characteristics consists of numerically integrating the equations of motion for inviscid supersonic flow by use of finite difference equations along Mach lines, where the equations reduce to ordinary differential equations. The equations programmed (on an IBM 7090 computer) for use in this investigation are those given by Hayes and Probstein in reference 9. The equations for the two families of Mach lines are

[1]The apparent divergence of some solutions in the transonic region near the body is still, at the writing of this report, being investigated.

$$\frac{dp}{\rho V^2 \tan \mu} \pm d\theta + \frac{\epsilon \sin \theta \sin \mu \, dx}{r \cos(\mu \pm \theta)} = 0 \qquad (2)$$

where $\epsilon = 1$ for axisymmetric flow and $\epsilon = 0$ for two-dimensional flow.

The flow is rotational behind the curved bow wave and the entropy varies from one streamline to another. The variation in entropy was calculated by linear interpolation between the streamlines. It is noted that this method can lead to difficulties if steep entropy gradients are encountered and the characteristic mesh is large. Under these conditions, continuity of mass between the free stream and the shock layer at any axial station may not be satisfied. In this investigation imbedded shock waves are not allowed in the flow field. The fluid may be either a perfect or a real gas in thermodynamic equilibrium. However, as noted earlier, Fuller's blunt-body solution is programmed for a perfect gas with a constant ratio of specific heats; therefore, the present calculations are limited to this case.

RESULTS AND DISCUSSION

The present method has been used to calculate the flow field around a number of blunt-nosed bodies for various values of free-stream Mach number and γ. The first example, flow of air for $M_\infty = 4.76$ over a hemisphere, is treated in some detail to illustrate the intermediate steps of the calculation method. The remaining examples include only the final results of shock-wave shape, surface-pressure distribution, and flow-field surveys that are compared with experimental data.

Example 1: Hemisphere, Air, $\gamma = 1.4$, $M_\infty = 4.76$

The first example considered is the flow field around a hemisphere. This example is mainly a test of the Fuller blunt-body solution, which was obtained with the assumption of a shock-wave shape with $B_s = 0.500$ and $A = -0.045$. The assumed shock-wave shape and the calculated body points and sonic line are shown in figure 1. The body points compare favorably with a circle defined by $\Delta/d = 0.0797$ and $d/R_S = 1.388$. The calculated sonic line is compared with the measurements of Kendall (ref. 10), who determined the sonic line location by measuring the termination of a shock wave generated by a small probe. Note that the measured points on the sonic line always lie within the theoretically subsonic region. This result may be peculiar to the measuring technique used by Kendall.

In order to continue the calculations in the supersonic region over the rest of the hemisphere, conditions were chosen on an appropriate line between the body and the shock wave. The 7 points indicated in figure 1 were used in the interpolation program to obtain 25 starting points for

the method of characteristics.[2] At the starting or matching point on the body, $x/d = 0.1318$ and $M = 1.04$, the body ordinate and slope differed from those for a hemisphere by 0.06 and 0.9 percent, respectively. The portion of the hemisphere after the matching point was represented by a fifth-degree polynomial with the ordinate, slope, and curvature at the end points used as boundary conditions.

The flow field over the supersonic portion of the hemisphere was then calculated by the method of characteristics. The calculated Mach number distribution on the hemisphere is shown in figure 2 and is compared with Kendall's data. In the region of the matching point between the blunt-body solution and the method of characteristics, $\varphi = 42.8^{\circ}$, the slope of the computed Mach number distribution is discontinuous. This discrepancy indicates that the Fuller blunt-body solution may be slightly in error in this region. Near the 90° point on the hemisphere, the experimental Mach numbers are lower than the calculated values. This may be due to viscous effects although Kendall points out that a three-to-fourfold change in Reynolds number had negligible effects on his measurements. In general, the present method appears to predict satisfactorily the flow field about a hemisphere.

Example 2: Hemisphere-Cylinder, Air, $\gamma = 1.4$, $M_{\infty} = 7.7$

The second example studied is a hemisphere with a cylindrical afterbody. This configuration has been the subject of numerous investigations including that of Kubota reported in reference 11. The shock-wave shape predicted by the present method is shown in figure 3 and is compared with Kubota's measurements. It is noted that the shock-wave shape is determined solely by the hemisphere since a characteristic line originating behind the hemisphere-cylinder juncture never intersects the shock wave. The calculated surface-pressure distribution is shown in figure 4 and is compared with the data. Near the hemisphere-cylinder juncture, the measured pressures are higher than the calculated values, corresponding to lower experimental Mach numbers found in the first example.

In figure 5 the calculated impact-pressure distribution between the body and the shock wave for $x/d = 3.0$ is compared with Kubota's measurements. Except for a layer near the surface where viscous effects are important, the results of the present inviscid flow-field calculations agree well with the measurements. The mass-flow rate between the body and the shock wave was calculated for $x/d = 5.0$ and was found to be 1 percent less than the mass-flow rate in the free stream. These comparisons show that the present calculation method predicts not only the surface-pressure distribution and shock-wave shape but also the variation of properties between the body and the shock wave.

[2]The use of 50 starting points in some other examples led to a large increase in computing time with no appreciable difference in the results.

Example 3: Hemisphere-Cylinder, Air, $\gamma = 1.4$, $M_\infty = 3.00$, 4.03, 5.06, 6.03, and 8.10

The experimental results of Baer (ref. 12) are used to test the present method over a range of Mach numbers.[3] In figure 6 the calculated shock-wave shapes for $M_\infty = 3.00$ to 6.03 are compared with the measured shapes. (The shock-wave shape was not measured for $M_\infty = 8.10$.) Comparisons between the calculated and measured pressure distributions for $M_\infty = 3.00$ to $M_\infty = 8.10$ are shown in figure 7 for the hemisphere and in figure 8 for the cylindrical afterbody. The effect of free-stream Mach number on the afterbody pressure distribution is of interest. For $M_\infty = 3.00$ the flow expands below free-stream pressure at the shoulder, and the pressure on the cylinder asymptotically approaches the free-stream value. For $M_\infty = 4.03$ the flow does not overexpand at the shoulder, but rather the pressure decreases to the free-stream value at $x/d = 1.7$ and reaches a minimum value at $x/d \sim 5$. For $M_\infty = 5.06$ and 6.03, the surface pressure decays to the free-stream value further downstream and does not reach a minimum within the model length of $l/d = 6.25$. For $M_\infty = 8.10$ the surface pressure always remains higher than the free-stream value within the model length. The pressures measured near the shoulder were higher than the calculated value for all Mach numbers except 3.00.

Example 4: Hemisphere-Cylinder, Helium, $\gamma = 1.6667$, $M_\infty = 15$ and 20

The flow of helium over hemisphere-cylinders is considered in this example. The shock-wave shapes calculated for $M_\infty = 15$ and 20 are shown in figure 9. Comparisons with measurements made in the Ames Hypersonic Helium Tunnel show good agreement not only in the nose region but far downstream. The good agreement is not unexpected in view of the previous comparisons for air. Hayes and Probstein point out in reference 9 that the effect of a change in γ on the flow field is opposite to that of Mach number; a flow with $\gamma = 1.6667$ and very large M_∞ is roughly equivalent to a flow with $\gamma = 1.4$ and $M_\infty \sim 3$.

Example 5: Sphere - 15°55' Cone-Cylinder, Air, $\gamma = 1.4$, $M_\infty = 4.95$

The preceding examples have been confined to hemisphere-cylinders. In this example, the present calculation method is applied to the blunted

[3]No comparisons are made with the data of reference 12 at $M_\infty = 1.99$ because the flow in the supersonic region was not obtained. Although the Fuller blunt-body solution could be found, the large extent of the subsonic region made it difficult to find an appropriate input line for the method of characteristics.

cone shown in figure 10. In order to obtain the flow field beyond the sharp corner between the cone and cylinder, the flow field properties were determined along a normal to the axis at the corner. A Prandtl-Meyer expansion was then used to obtain new flow properties on the body slightly downstream on the cylinder. These properties were then used as input points to the method of characteristics to obtain the solution downstream of the corner. The calculated surface-pressure distribution is shown in figure 10 and shows good agreement with the measurements of McConnell (ref. 13).

Example 6: Blunt Ellipsoid-Cylinder, Air, $\gamma = 1.4$, $M_\infty = 5.12$

To demonstrate the present method for a nose shape other than a sphere, the flow field has been calculated for a cylinder with a blunt ellipsoidal nose defined by the following equation:

$$\left(1 - 4\,\frac{x}{d}\right)^{2.5} + \left(2\,\frac{r}{d}\right)^{2} = 1 \qquad (3)$$

Good agreement is shown in figure 11 between the predicted shock-wave shape ($B_S = 1.30$, $A = 0.40$) and the measurements from a shadowgraph of a free-flight model.

Example 7: Flat Plate With Circular Cylindrical Leading Edge, Air, $\gamma = 1.4$, $M_\infty = 4.70$

The preceding examples have been concerned with axisymmetric bodies. The two-dimensional problem is more difficult because of the large extent of the subsonic region. As a result, Fuller's solution becomes more difficult to obtain. In addition, for a given body profile, the flow does not expand as rapidly around the nose, and any small error in the body input point may result in an imbedded shock wave.

A simple blunt two-dimensional body is a flat plate with a circular cylindrical leading edge, which has been investigated experimentally in some detail by Tendeland, Nielsen, and Fohrman as reported in reference 14. The calculated shock-wave shape shown in figure 12 and the surface-pressure distributions shown in figure 13 compare favorably with the results of reference 14. Note that the calculations do not take into consideration the boundary layer and, hence, predict surface pressures that are lower than the measurements.

A number of static- and impact-pressure surveys were taken in the tests of reference 14, but none of those reported extend out to the shock wave. In figure 14, unpublished impact-pressure surveys for $x/d = 26.2$ and 50.0 and a leading-edge diameter of 1/8 inch are compared with the calculated impact-pressure distributions. Near the wall, the measured impact pressures are lower because of the strong viscous effects. However, for the outer 80 percent of the distance between the body and the shock wave, the impact pressure is predicted by inviscid theory.[4] A check on the mass-flow rate showed that continuity of mass between the free stream and the shock layer at $x/d = 50$ was satisfied within 1 percent. It is significant that even at this large distance from the leading edge, the flow properties are not constant between the body and the shock wave.

Example 8: Sphere - 18° Cone, Air, $M_\infty = 17.8$

Since the present calculations are limited to a perfect gas, the real gas case is treated approximately with the assumption of an effective value of γ behind the shock wave. In figure 15 the shock-wave shape determined from a shadowgraph of a blunted cone fired in the Ames Supersonic Free-Flight Wind Tunnel is compared with shock-wave shapes calculated for $\gamma = 1.24$ and 1.32. For the given test conditions, the value of γ at the stagnation point was determined to be 1.24 with the thermodynamic properties of air given in references 15 and 16. In the nose region, good agreement is obtained between the measured and calculated shock shapes for $\gamma = 1.24$; but downstream, better agreement is obtained for $\gamma = 1.32$. The calculated drag coefficient, with base drag neglected, was 30 percent lower than the measured value of 0.166. The higher measured drag was partly due to model pitching.

SUMMARY OF RESULTS

The inviscid flow of a perfect gas at zero angle of attack over blunt-nosed axisymmetric and two-dimensional bodies has been calculated numerically on an IBM 7090 computer. The method of calculation consisted of the Fuller blunt-body solution for the subsonic and transonic regions and the method of characteristics for the supersonic region. The following results were obtained:

1. For the flow of a perfect gas, the results of the present calculation method agreed well with experimental shock-wave shapes, surface-pressure distributions, and flow-field surveys.

[4]The two disturbances in the outer portion of the shock layer for $x/d = 50$ are shock waves emanating from the boundary-layer trip.

2. For a case where real gas effects were significant, the shock-wave shape was predicted well with a perfect gas solution calculated with the value of γ at the stagnation point.

Ames Research Center
National Aeronautics and Space Administration
Moffett Field, Calif., June 21, 1962

REFERENCES

1. Gravalos, F. G., Edelfelt, I. H., and Emmons, H. W.: The Supersonic Flow About a Blunt Body of Revolution for Gases at Chemical Equilibrium. Proc. IX International Astronautical Congress, Amsterdam, vol. 1, Aug. 25-30, 1958, pp. 312-322.

2. Feldman, Saul: Numerical Comparison Between Exact and Approximate Theories of Hypersonic Inviscid Flow Past Slender Blunt-Nosed Bodies. ARS Journal, vol. 30, no. 5, May 1960, pp. 463-468.

3. Vaglio-Laurin, Roberto, and Trella, Massimo: A Study of Flow Fields About Some Typical Blunt-Nosed Slender Bodies. PIBAL Rep. no. 623, Polytechnic Inst. of Brooklyn, Dept. of Aerospace Engr. and Applied Mech., 1960.

4. Martellucci, Anthony: Real Gas Characteristics Analysis for the Flow About a Blunted Axisymmetric Cone. Tech. Rep. no. 162, General Applied Science Laboratories, Inc., May 1960.

5. Capiaux, R., and Karchmar, L.: Flow Past Slender Blunt Bodies - A Review and Extension. IAS Paper no. 61-210-1904, June 1961.

6. Fuller, Franklyn B.: Numerical Solutions for Supersonic Flow of an Ideal Gas Around Blunt Two-Dimensional Bodies. NASA TN D-791, 1961.

7. Van Dyke, Milton D.: The Supersonic Blunt-Body Problem - Review and Extension. Journal of the Aero/Space Sciences, vol. 25, no. 8, Aug. 1958, pp. 485-496.

8. Van Dyke, Milton D., and Gordon, Helen D.: Supersonic Flow Past a Family of Blunt Axisymmetric Bodies. NASA TR R-1, 1959.

9. Hayes, Wallace D., and Probstein, Ronald F.: Hypersonic Flow Theory. Academic Press, New York, 1959, pp. 202-210, 253-258.

10. Kendall, James M., Jr.: Experiments on Supersonic Blunt-Body Flows. Prog. Rep. 20-372, Jet Propulsion Lab., Calif. Institute of Tech., Feb. 1959.

11. Kubota, Toshi: Investigation of Flow Around Simple Bodies in Hypersonic Flow. GALCIT Memo, no. 40, June 25, 1957.

12. Baer, A. L.: Pressure Distributions on a Hemisphere Cylinder at Supersonic and Hypersonic Mach Numbers. AEDC TN-61-96, Arnold Engineering Development Center, 1961.

13. McConnell, Dudley George: Free-Flight Observation of a Separated Turbulent Flow Including Heat Transfer Up to Mach 8.5. NASA TN D-278, 1961.

14. Tendeland, Thorval, Nielsen, Helmer L., and Fohrman, Melvin J.: The Flow Field Over Blunted Flat Plates and Its Effect on Turbulent Boundary-Layer Growth and Heat Transfer at a Mach Number of 4.7. NASA TN D-689, 1961.

15. Moeckel, W. E., and Weston, Kenneth C.: Composition and Thermodynamic Properties of Air in Chemical Equilibrium. NACA TN 4265, 1958.

16. Hansen, C. Frederick: Approximations for the Thermodynamic and Transport Properties of High-Temperature Air. NASA TR R-50, 1959.

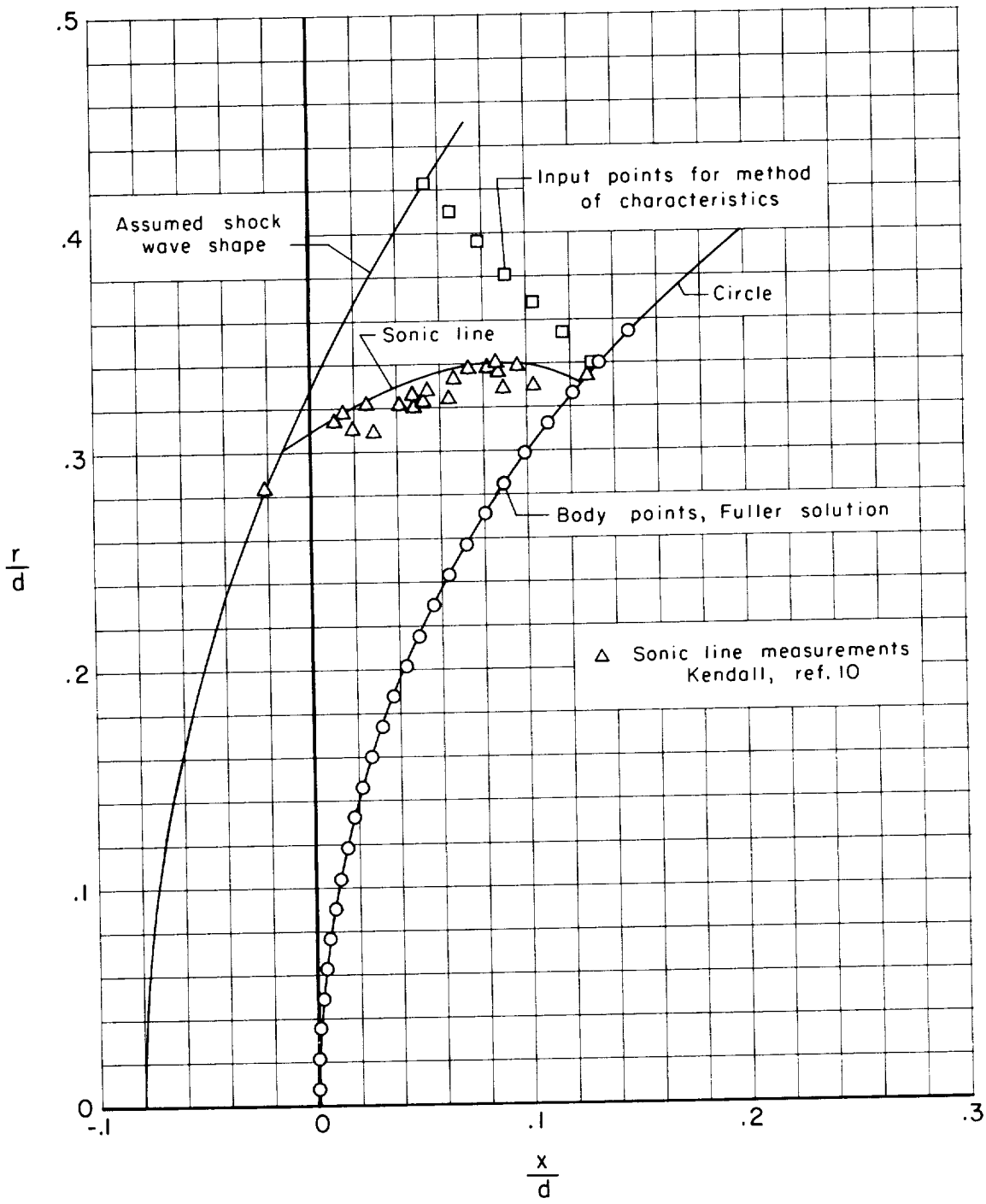

Figure 1.- Shock-wave shape and sonic line for hemisphere; $\gamma = 1.4$, $M_\infty = 4.76$.

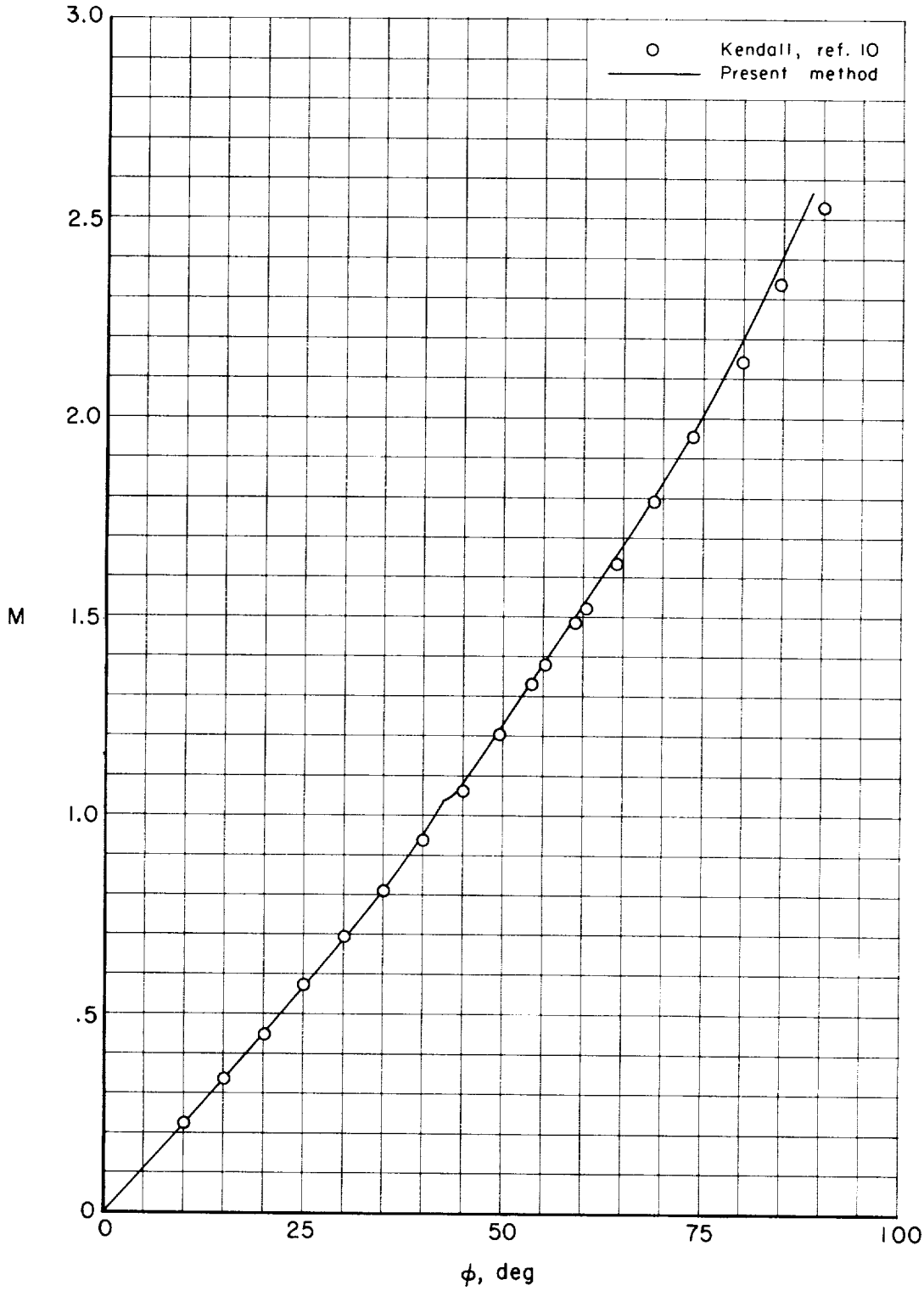

Figure 2.- Mach number distribution on hemisphere; $\gamma = 1.4$, $M_\infty = 4.76$.

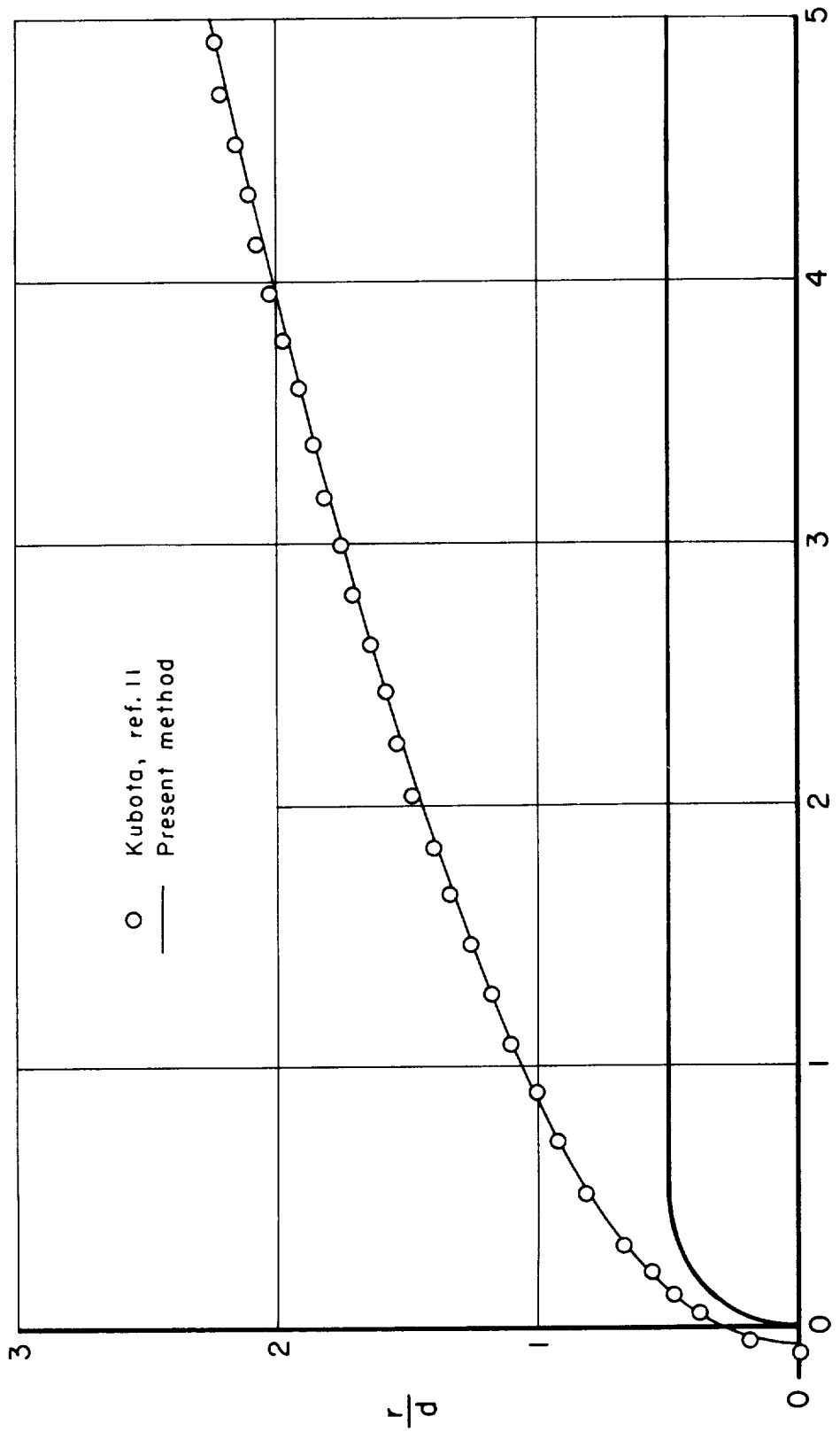

Figure 3.- Shock-wave shape for hemisphere-cylinder; $\gamma = 1.4$, $M_\infty = 7.7$.

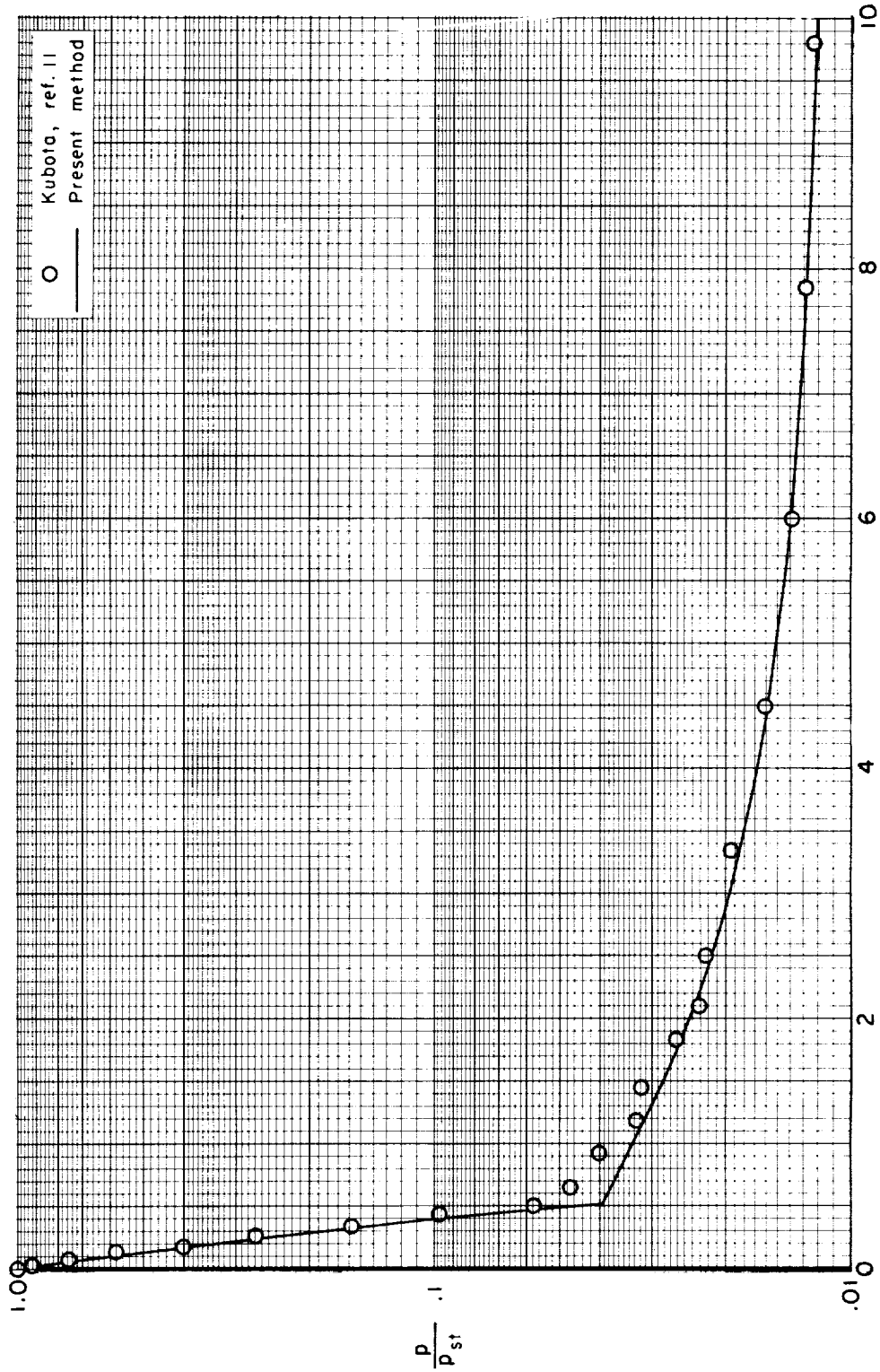

Figure 4.- Surface-pressure distribution on hemisphere-cylinder; $\gamma = 1.4$, $M_\infty = 7.7$.

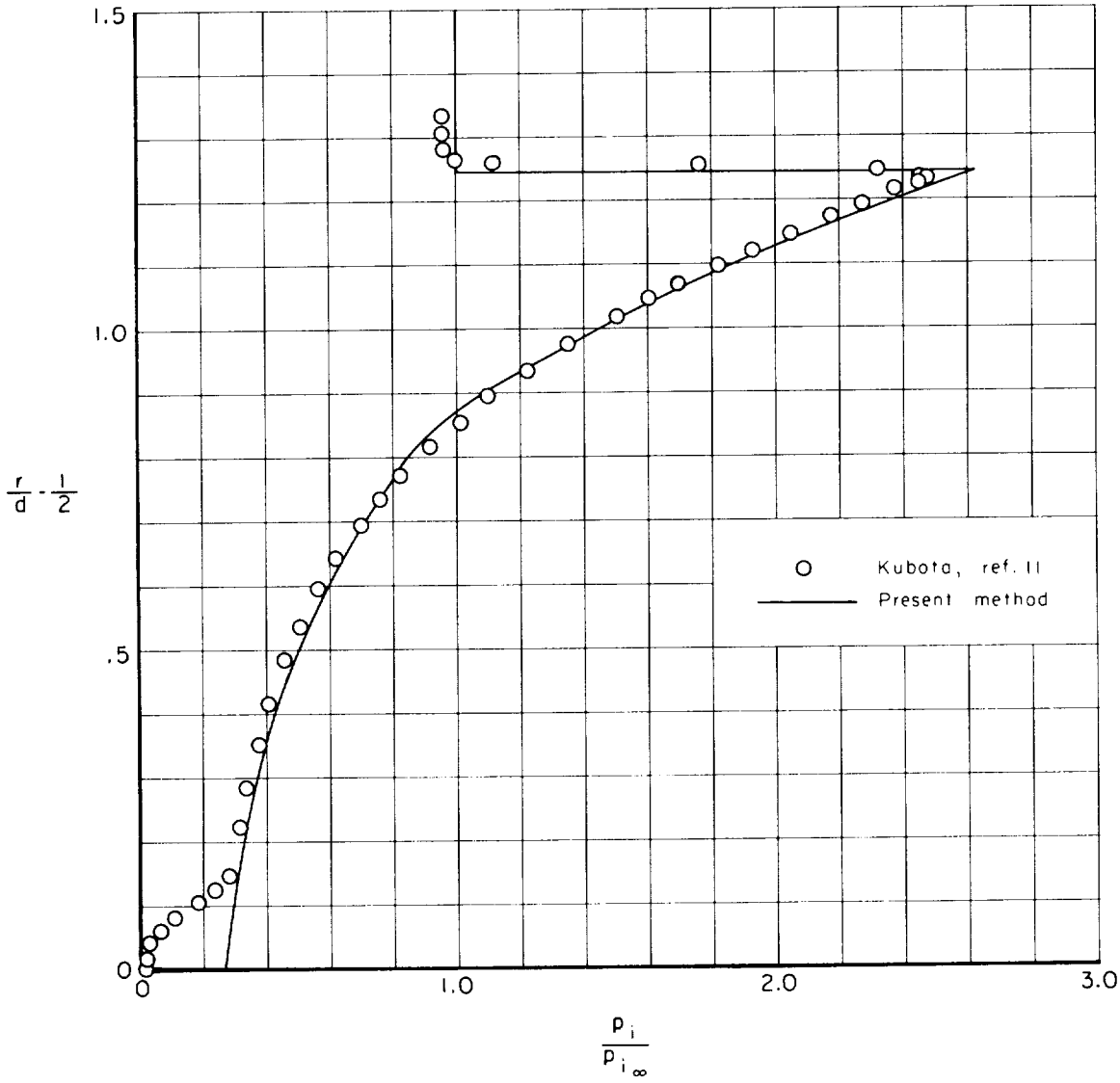

Figure 5.- Impact-pressure distribution between hemisphere-cylinder and shock wave; $\gamma = 1.4$, $M_\infty = 7.7$, $x/d = 3.0$.

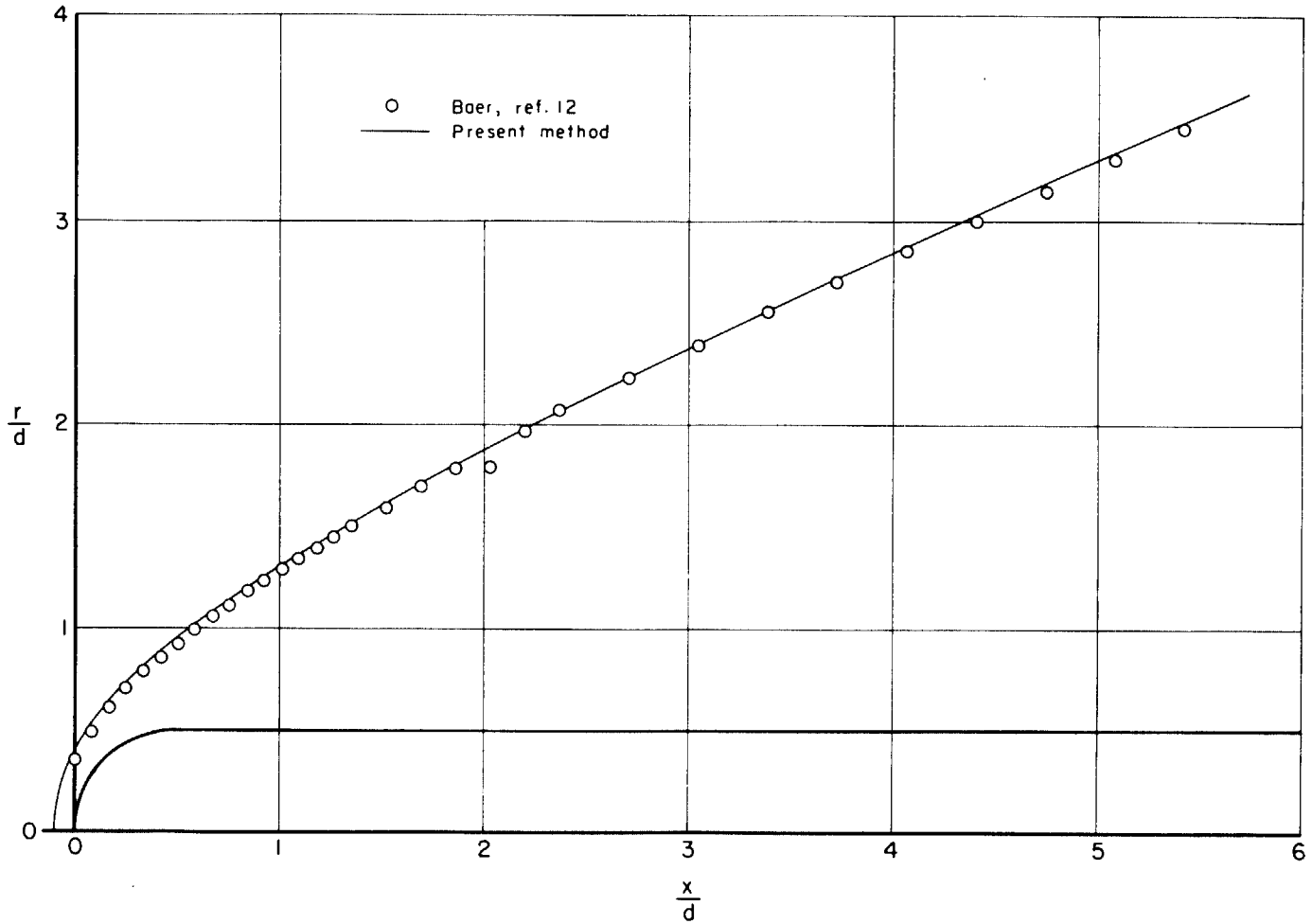

(a) $M_\infty = 3.00$, $Re_\infty = 2.0 \times 10^6$

Figure 6.- Shock-wave shape for hemisphere-cylinder; $\gamma = 1.4$.

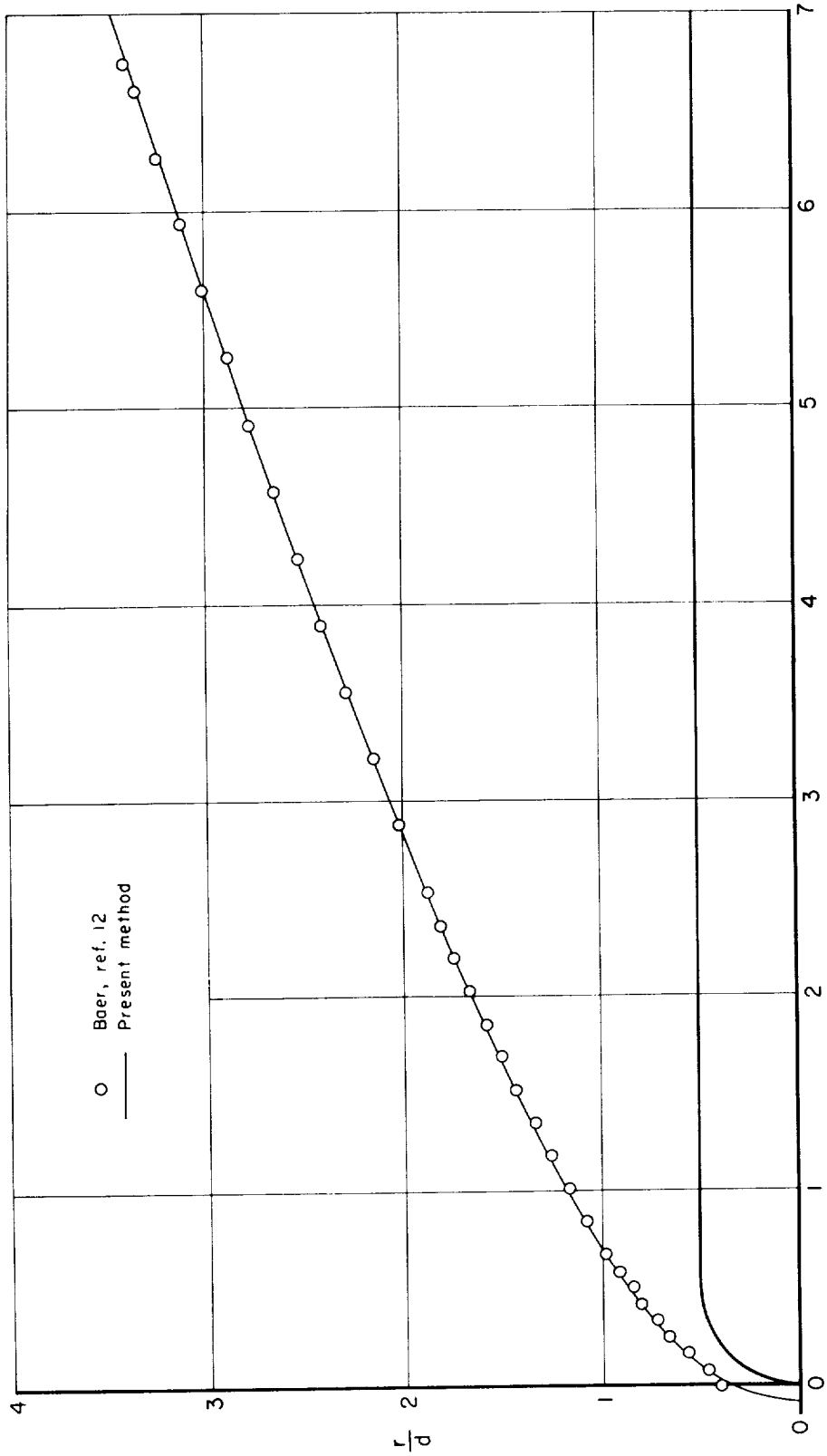

(b) $M_\infty = 4.03$, $Re_\infty = 2.6 \times 10^6$

Figure 6.- Continued.

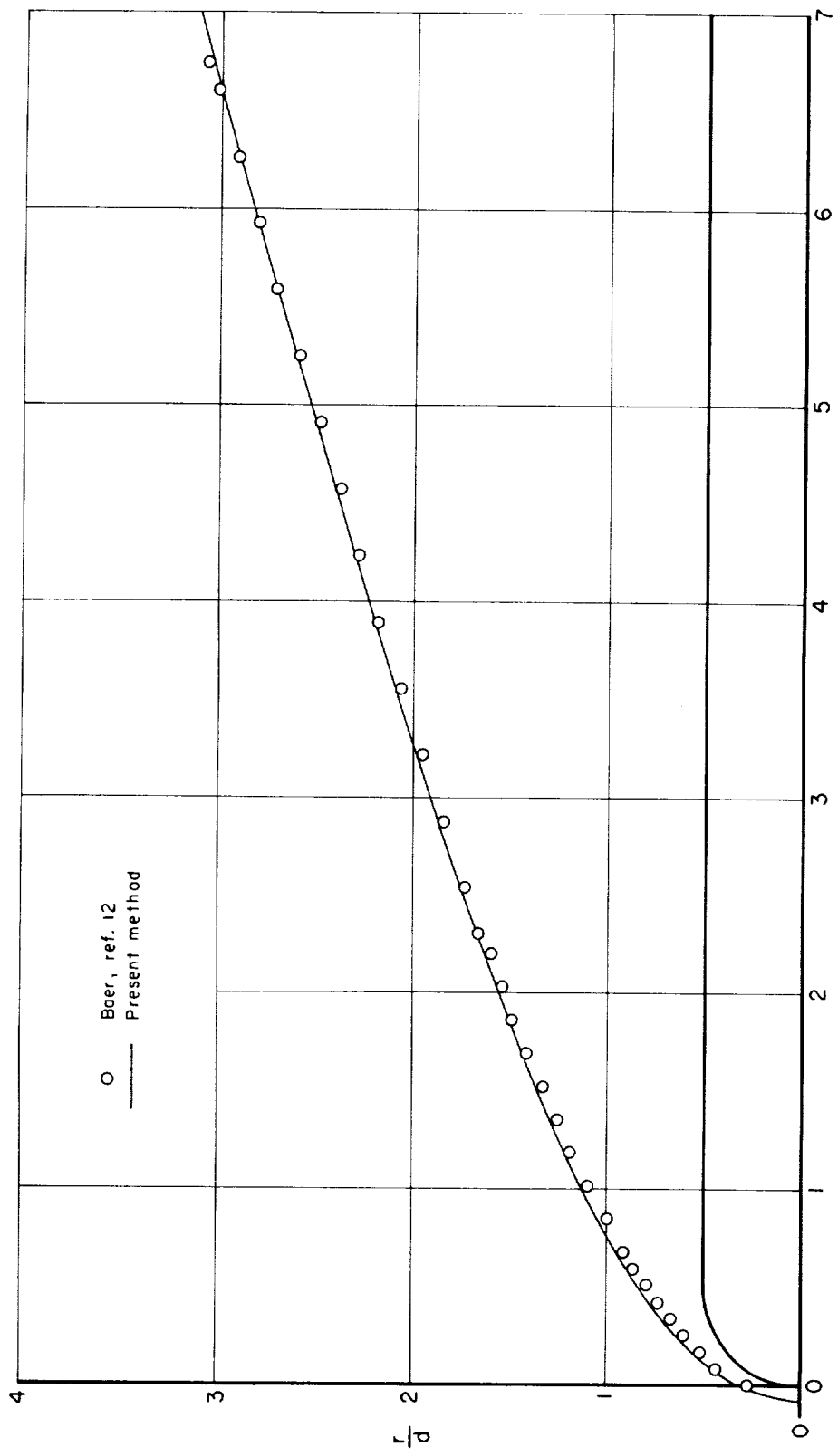

(c) $M_\infty = 5.06$, $Re_\infty = 3.0 \times 10^6$

Figure 6.- Continued.

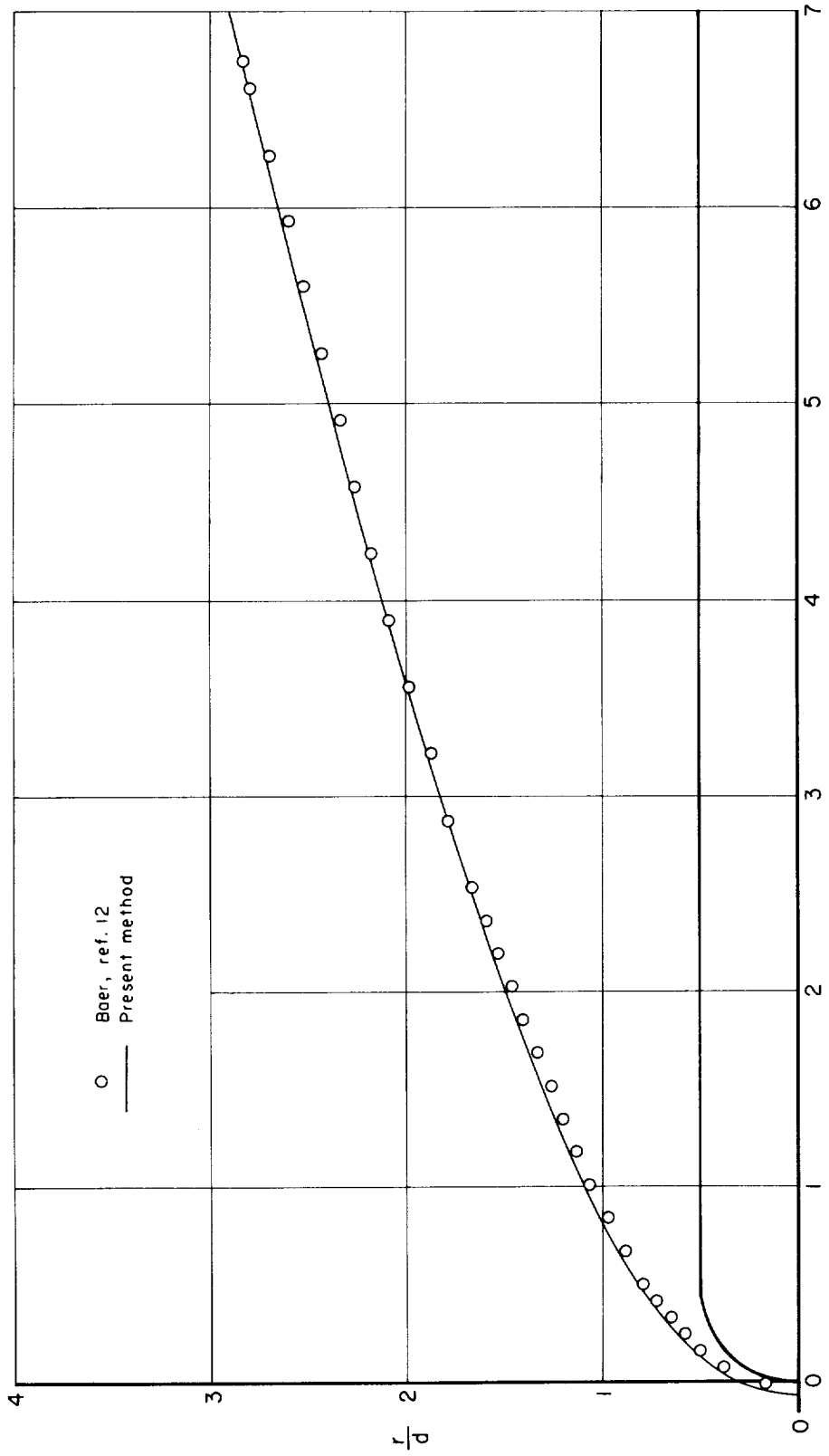

(d) $M_\infty = 6.03$, $Re_\infty = 2.2 \times 10^8$

Figure 6.- Concluded.

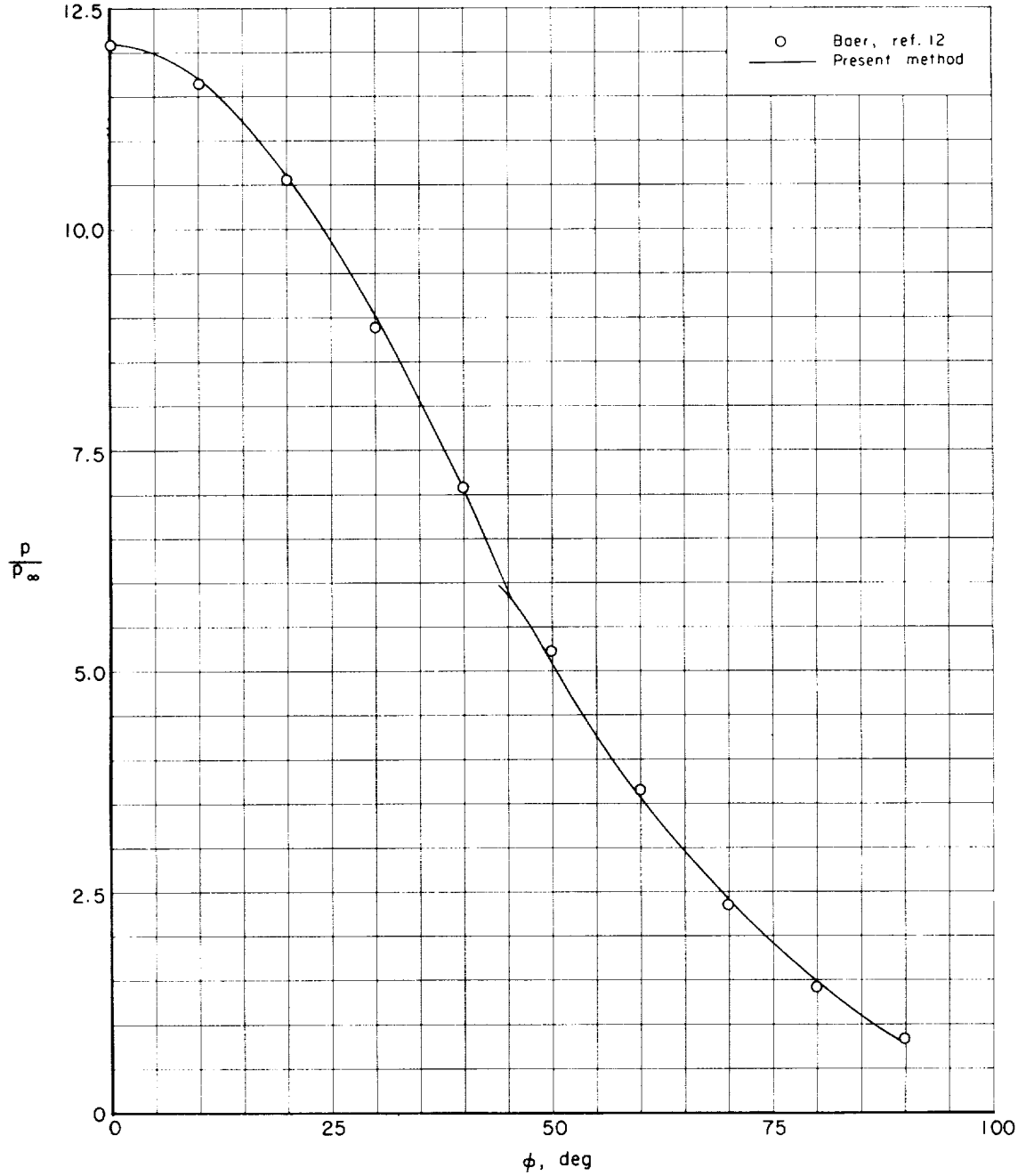

(a) $M_\infty = 3.0$, $Re_\infty = 2.0 \times 10^6$

Figure 7.- Surface-pressure distribution on hemisphere; $\gamma = 1.4$.

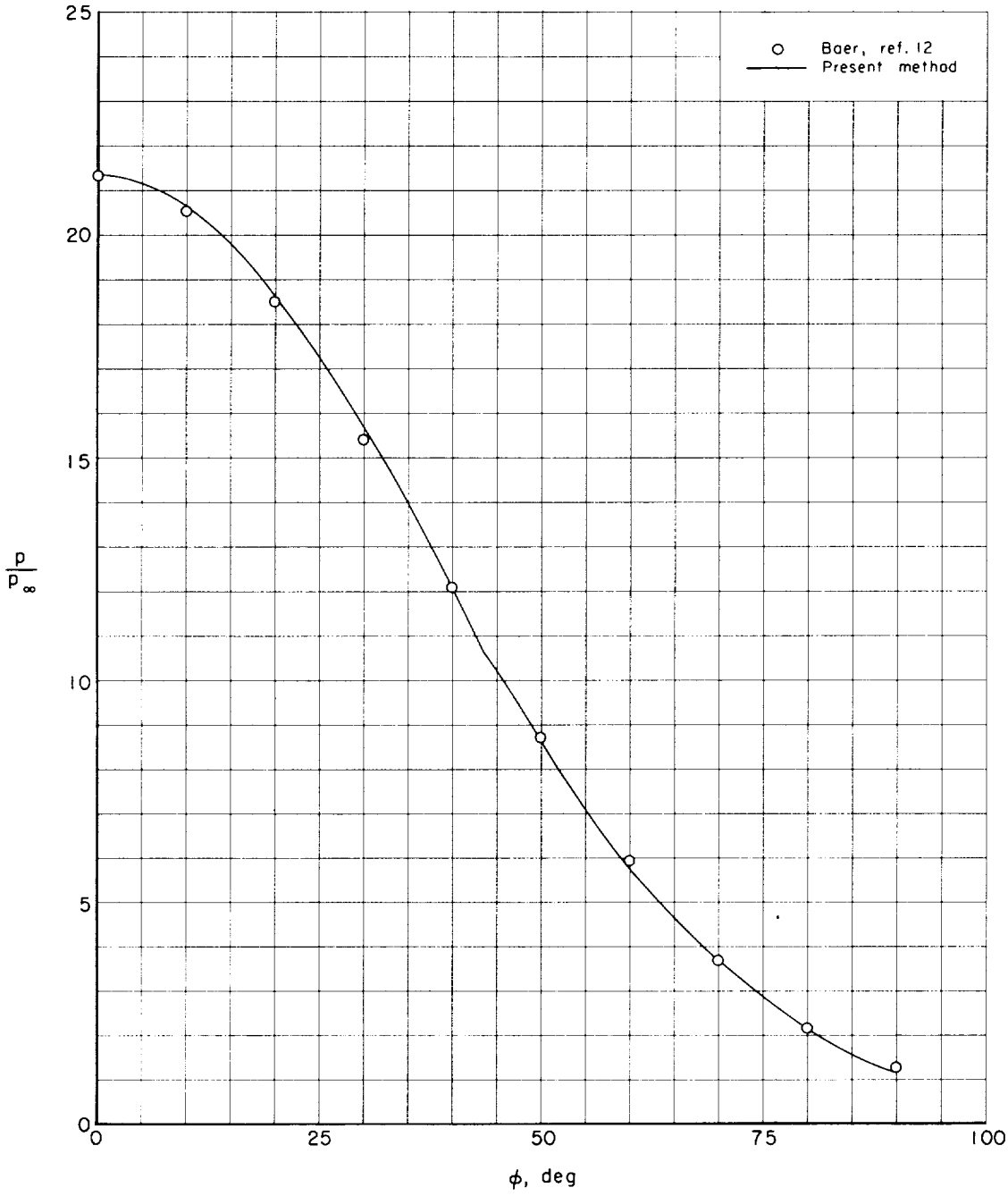

(b) $M_\infty = 4.03$, $Re_\infty = 2.6 \times 10^6$

Figure 7.- Continued.

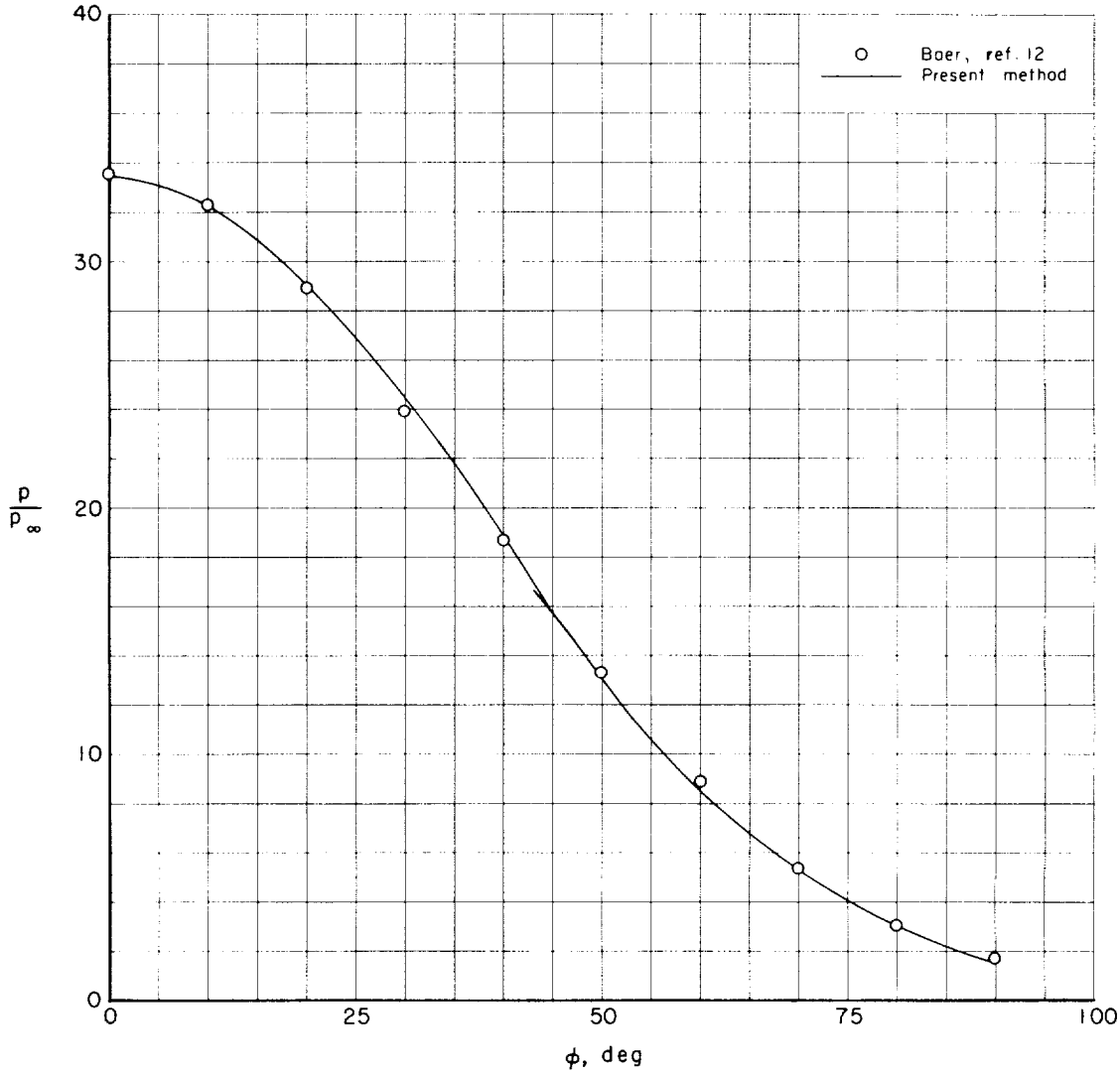

(c) $M_\infty = 5.06$, $Re_\infty = 3.0 \times 10^6$

Figure 7.- Continued.

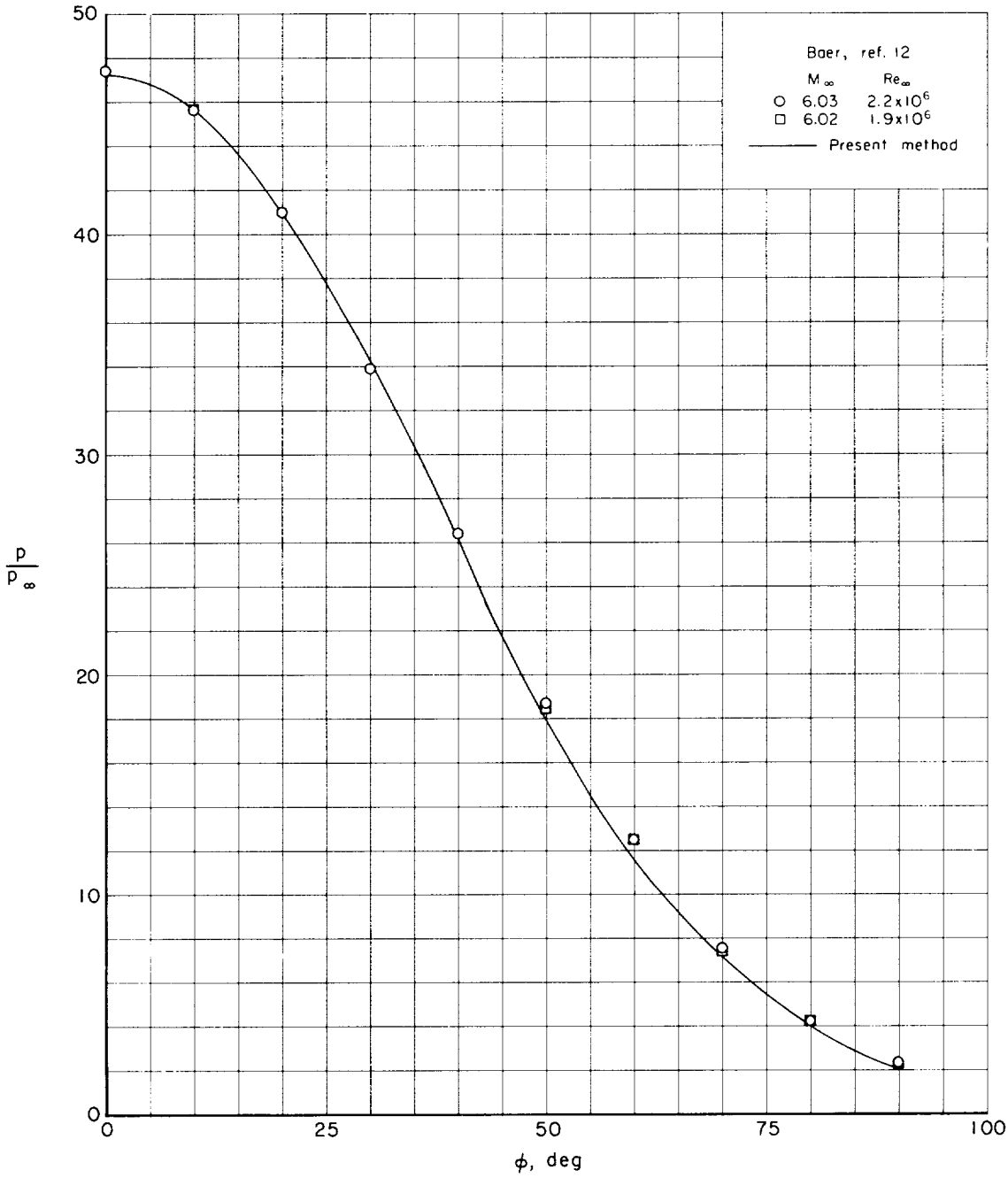

(d) $M_\infty = 6.03$

Figure 7.- Continued.

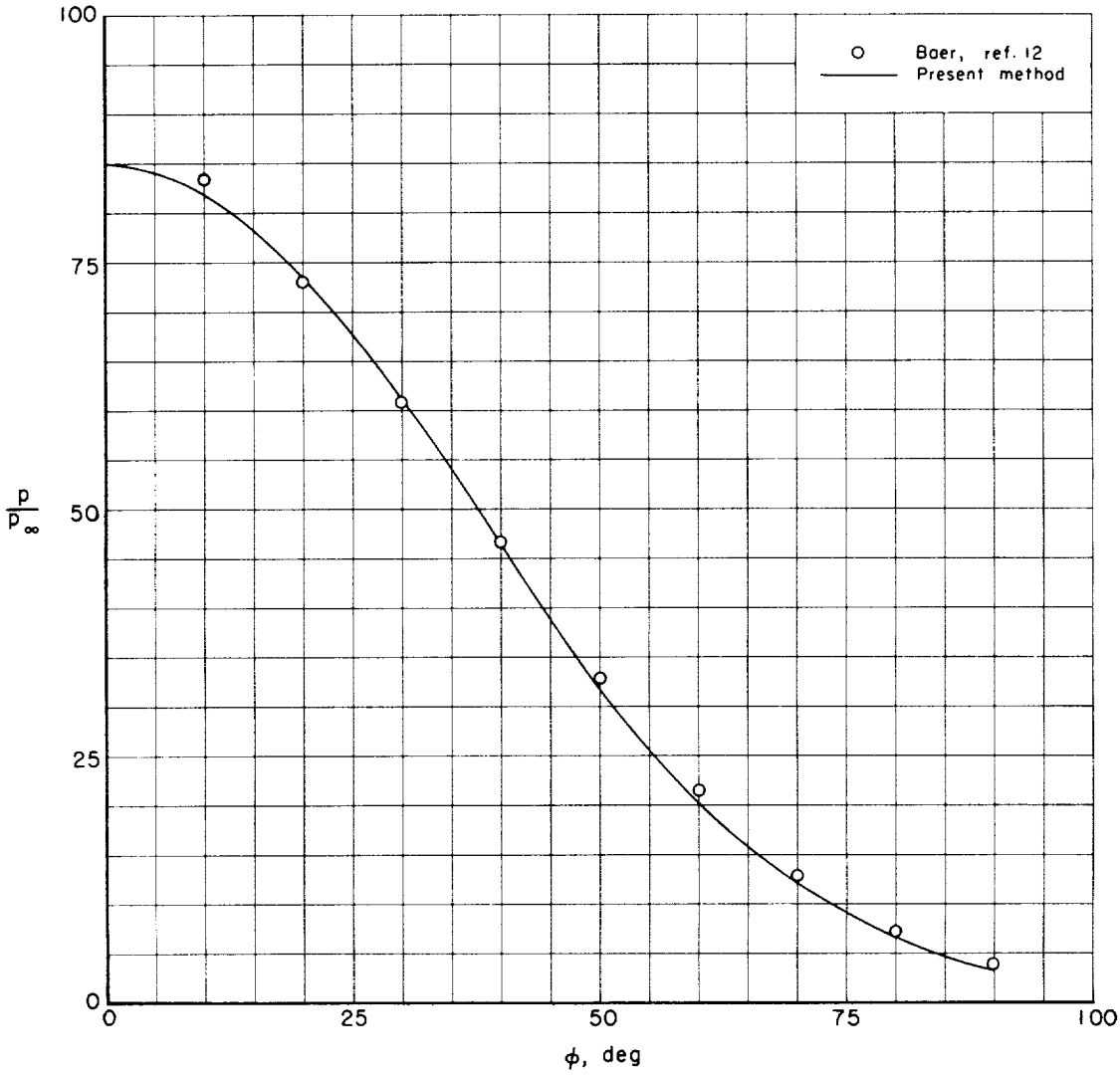

(e) $M_\infty = 8.10$, $Re_\infty = 1.3 \times 10^6$

Figure 7.- Concluded.

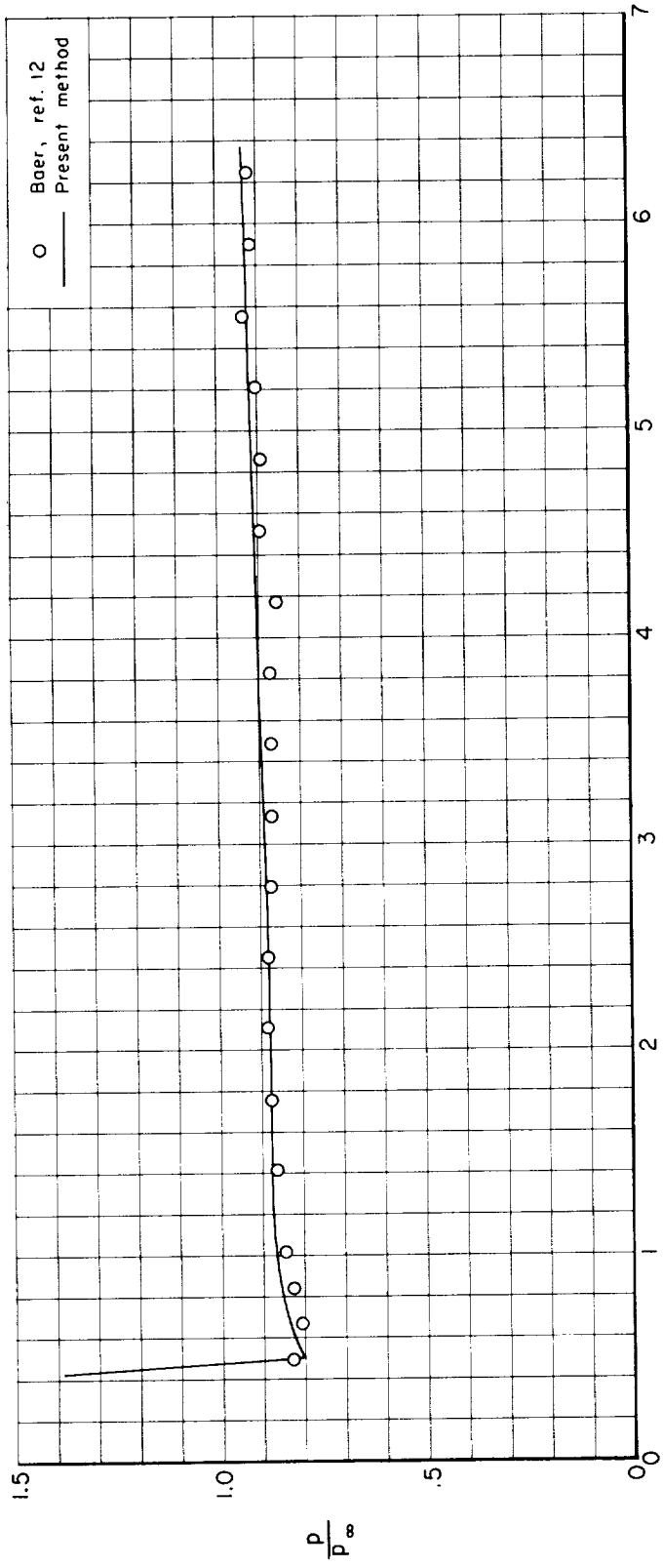

(a) $M_\infty = 3.00$, $Re_\infty = 2.0 \times 10^6$

Figure 8.- Surface-pressure distribution on cylindrical afterbody; $\gamma = 1.4$.

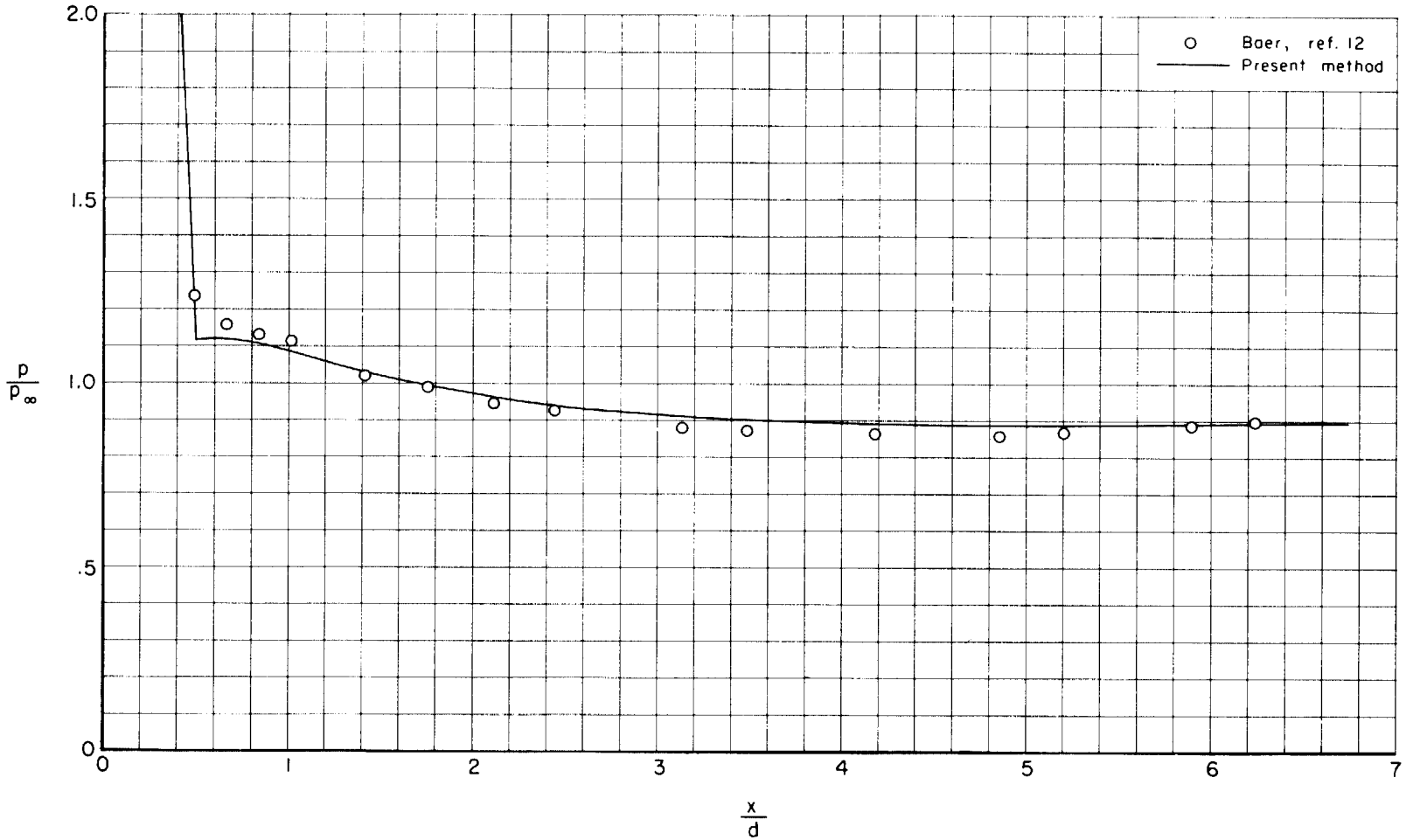

(b) $M_\infty = 4.03$, $Re_\infty = 2.6 \times 10^6$

Figure 8.- Continued.

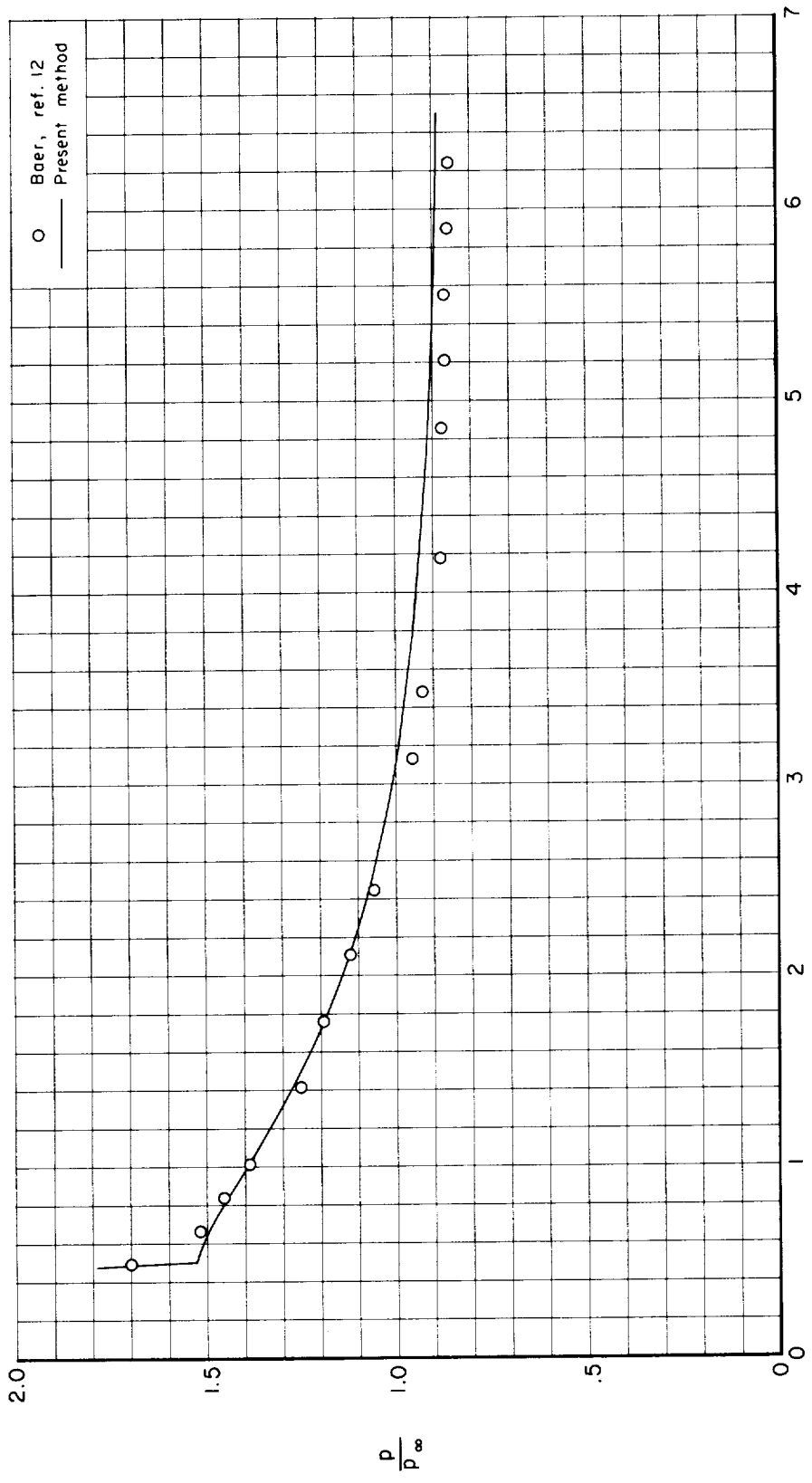

(c) $M_\infty = 5.06$, $Re_\infty = 3.0 \times 10^6$

Figure 8.- Continued.

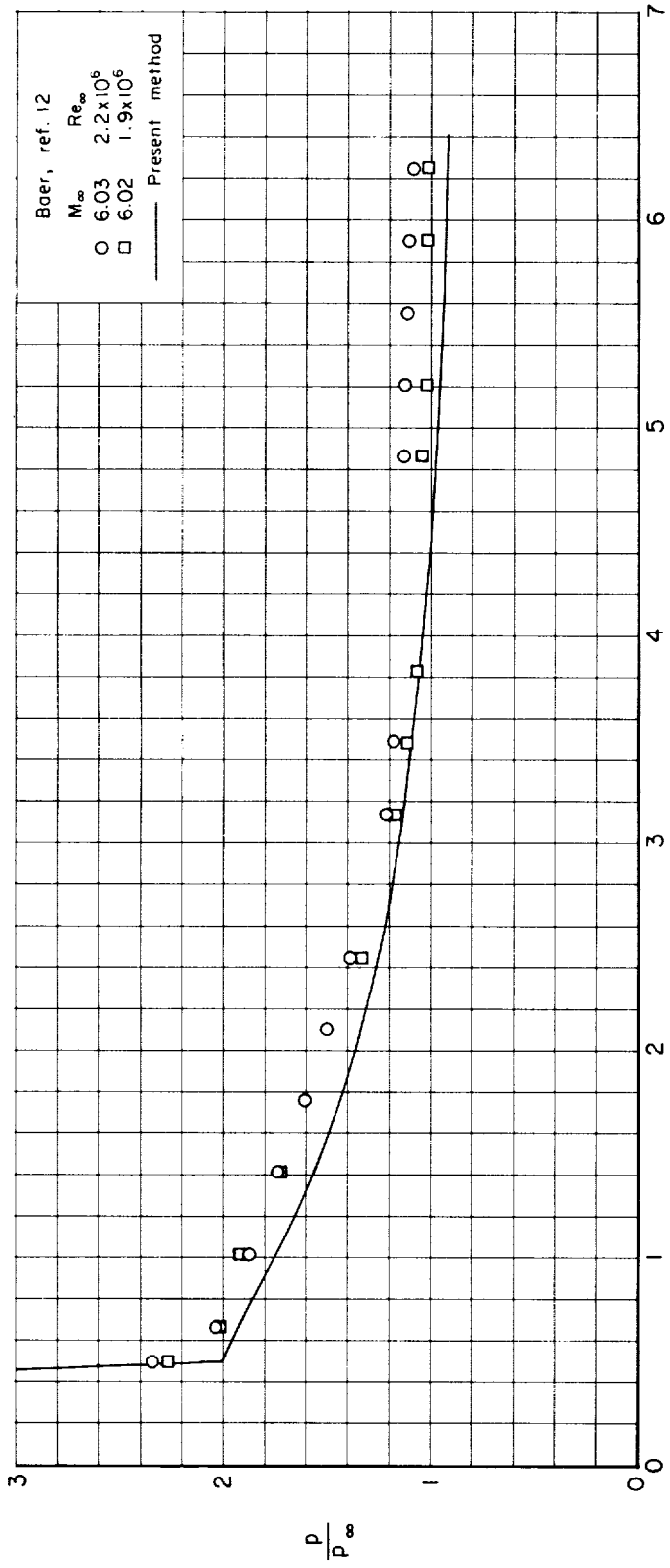

(d) $M_\infty = 6.03$

Figure 8.- Continued.

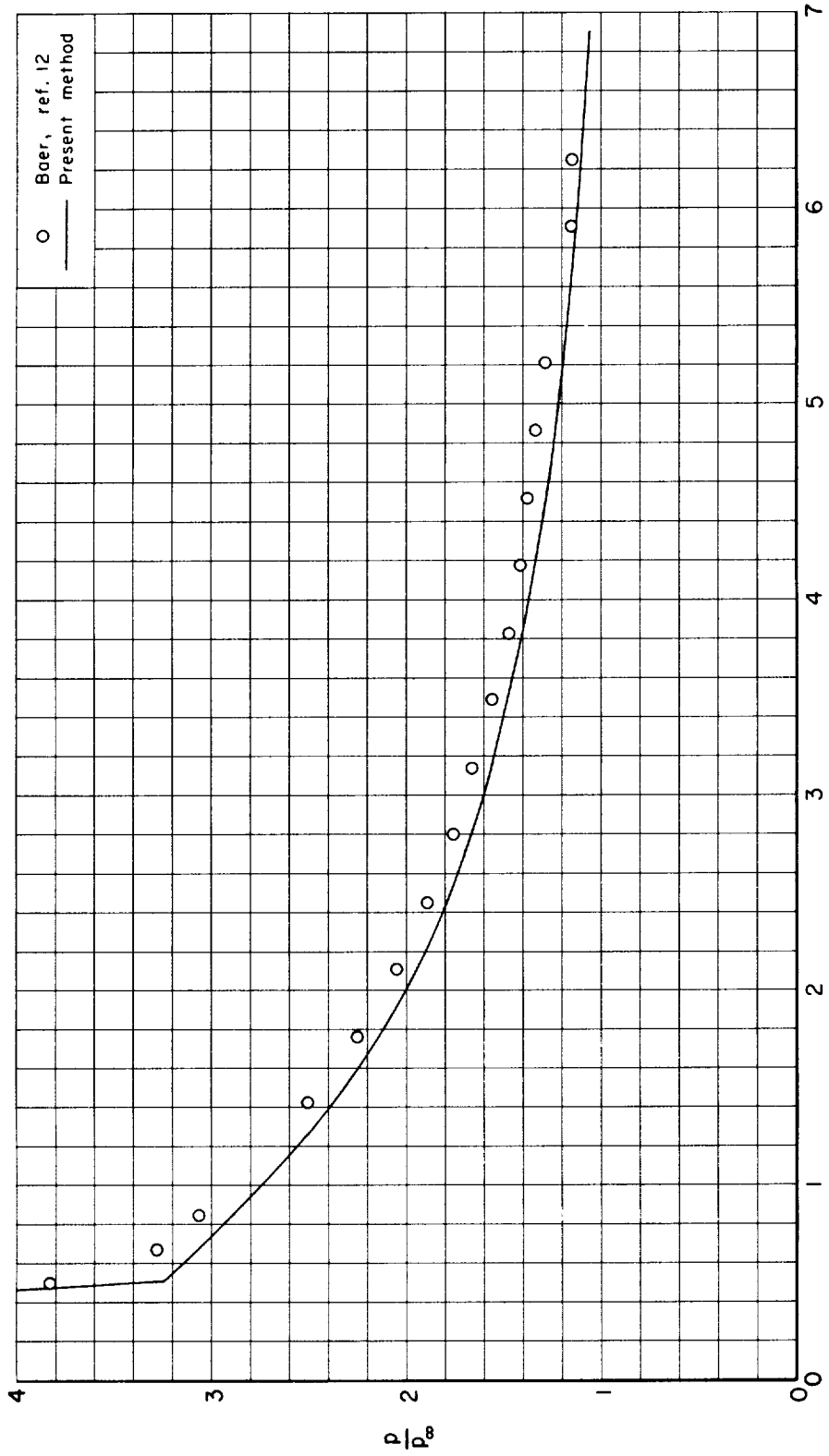

(e) $M_\infty = 8.10$, $Re_\infty = 1.3 \times 10^6$

Figure 8.- Concluded.

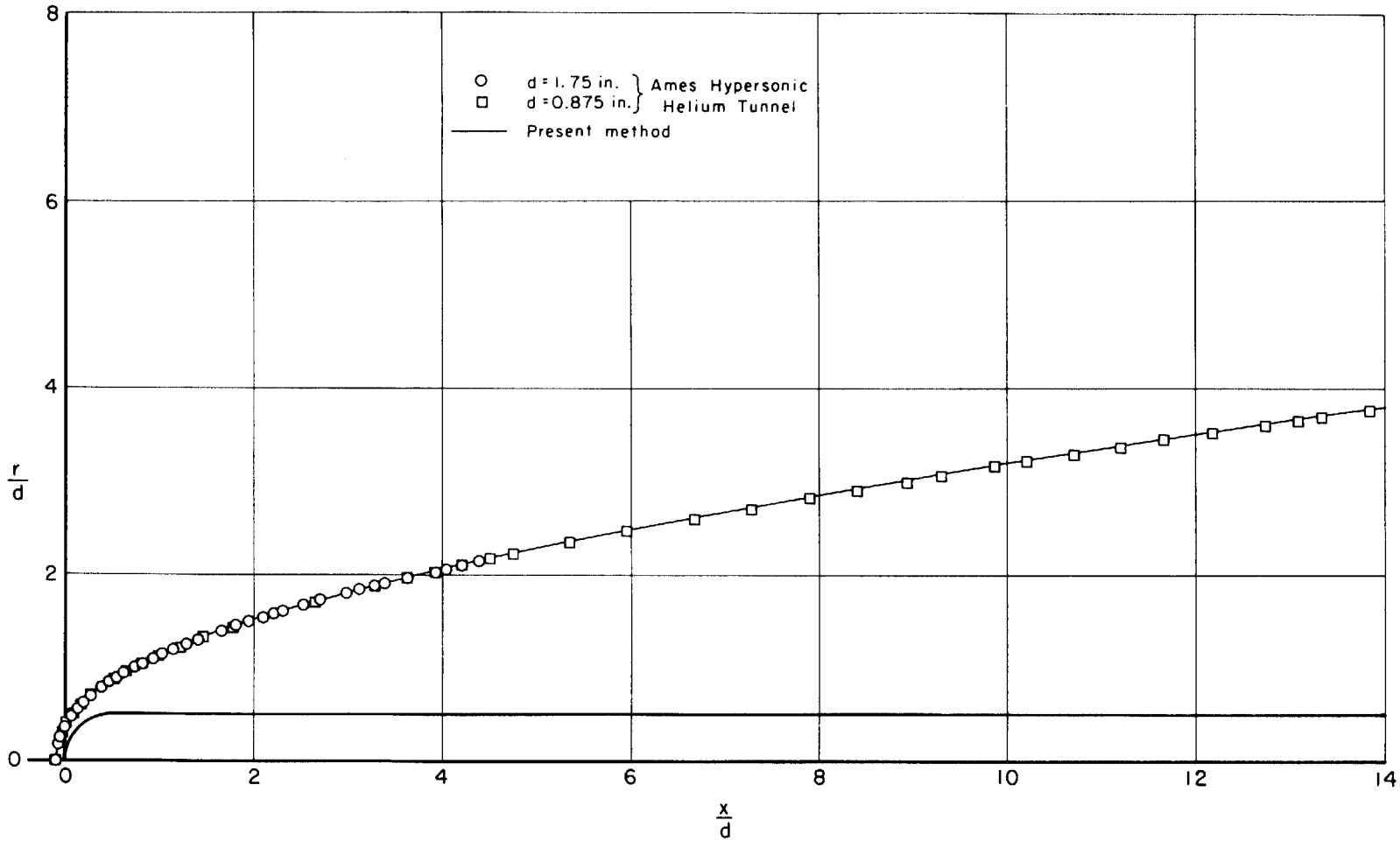

(a) $M_\infty = 15$

Figure 9.- Shock-wave shape for hemisphere-cylinder; $\gamma = 1.6667$.

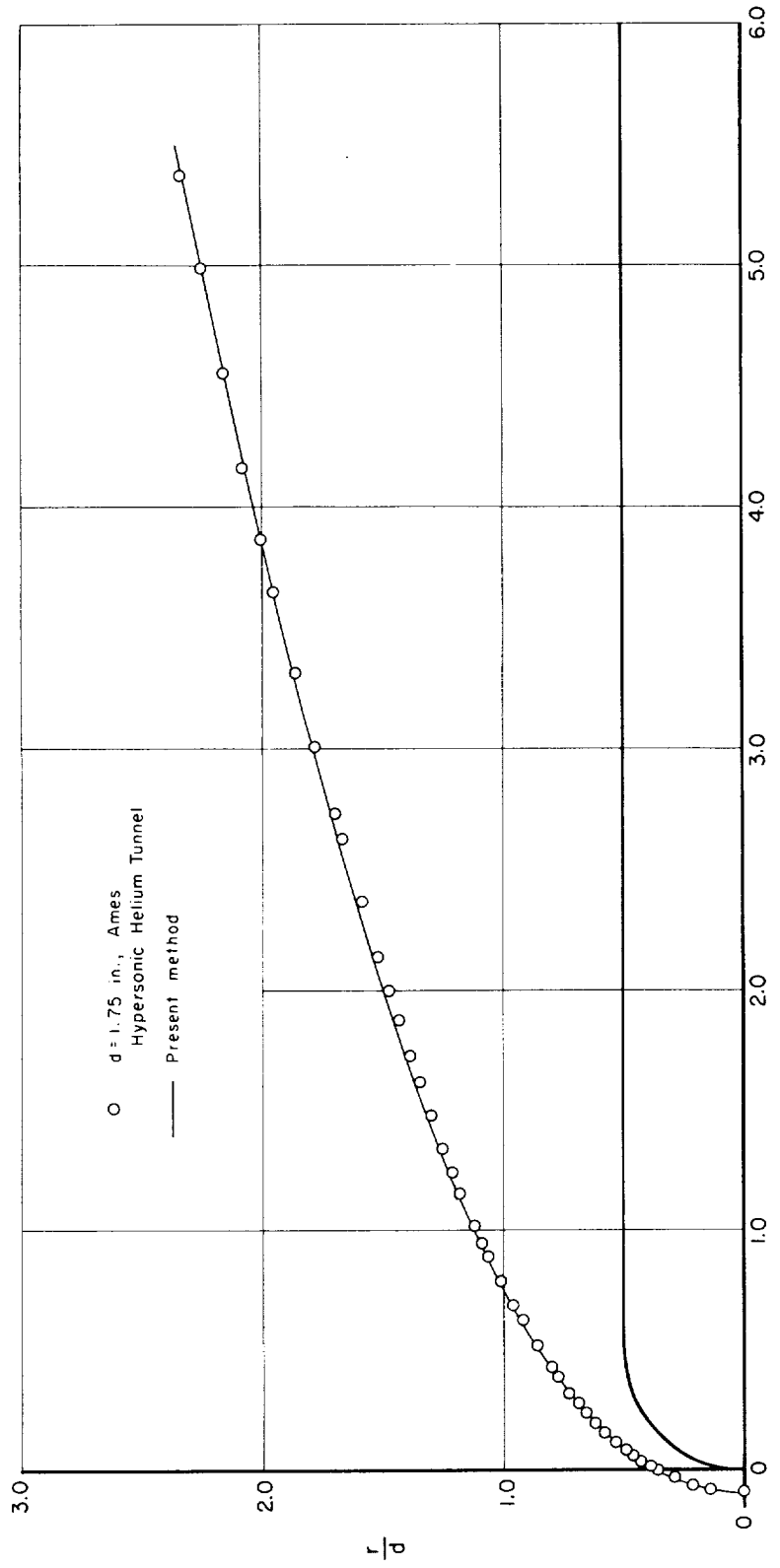

(b) $M_\infty = 20$

Figure 9.- Concluded.

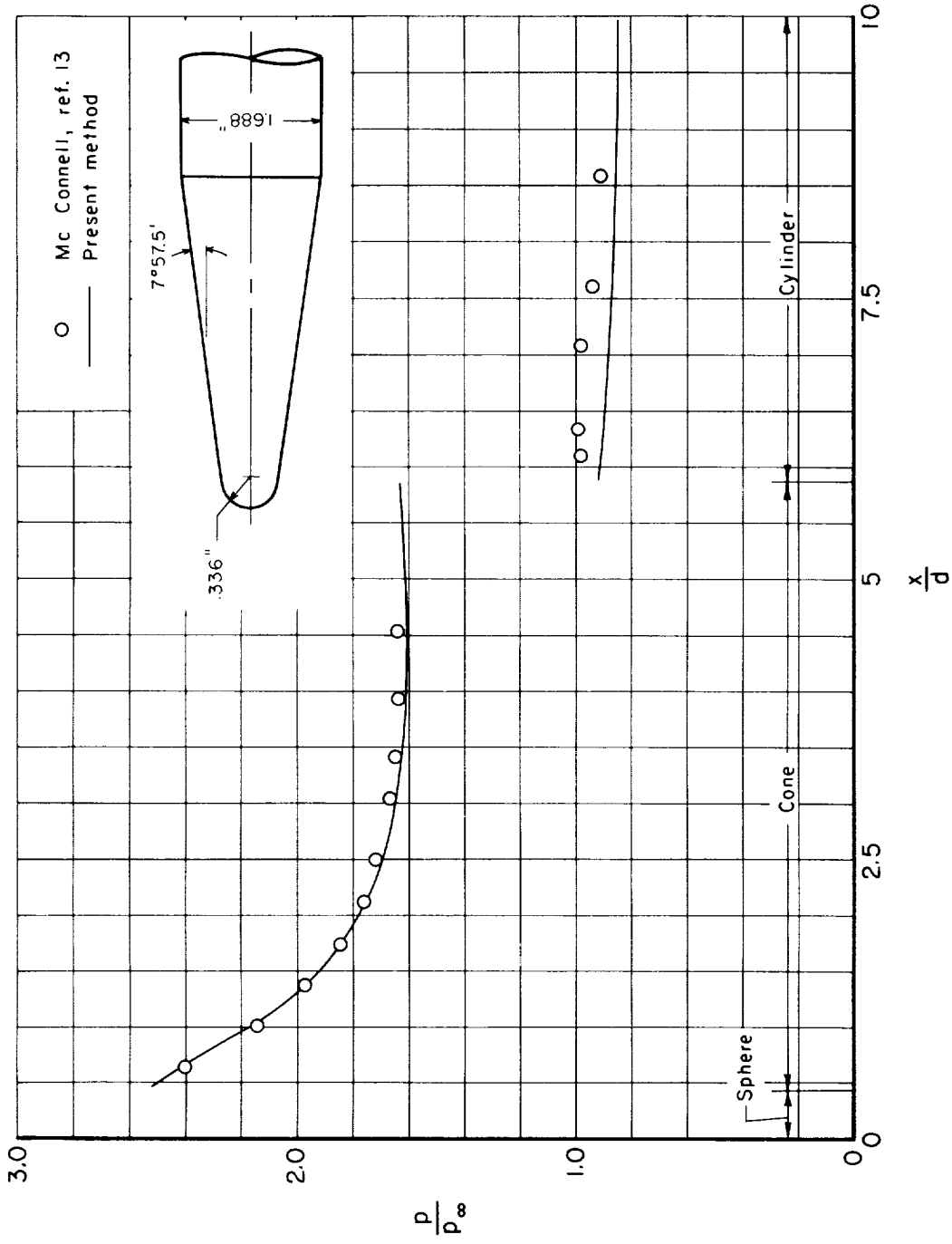

Figure 10.- Surface-pressure distribution on sphere-15°55' cone; $\gamma = 1.4$, $M_\infty = 4.95$, d = 0.672 inch.

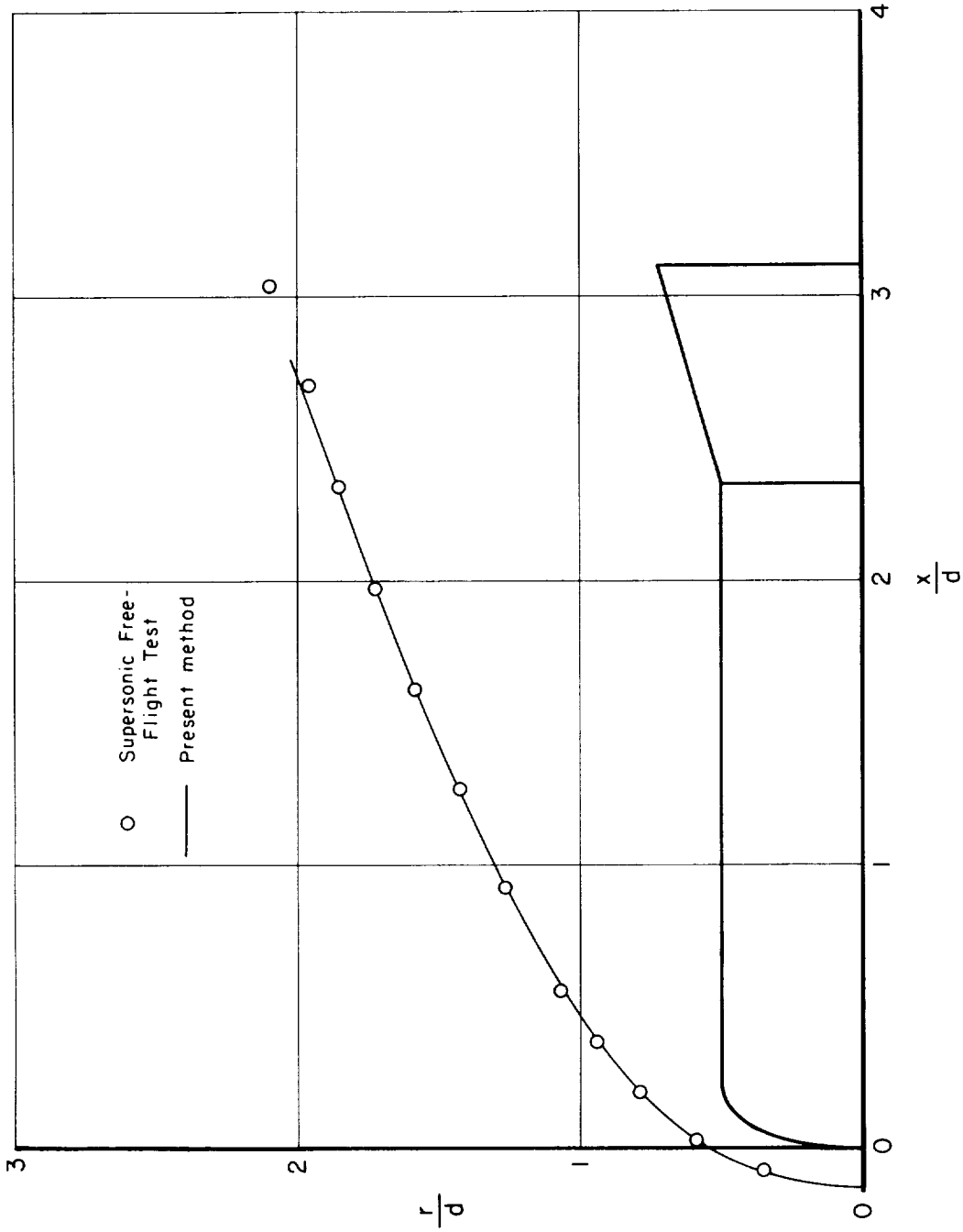

Figure 11.- Shock-wave shape for blunt ellipsoid-cylinder; $\gamma = 1.4$, $M_\infty = 5.12$.

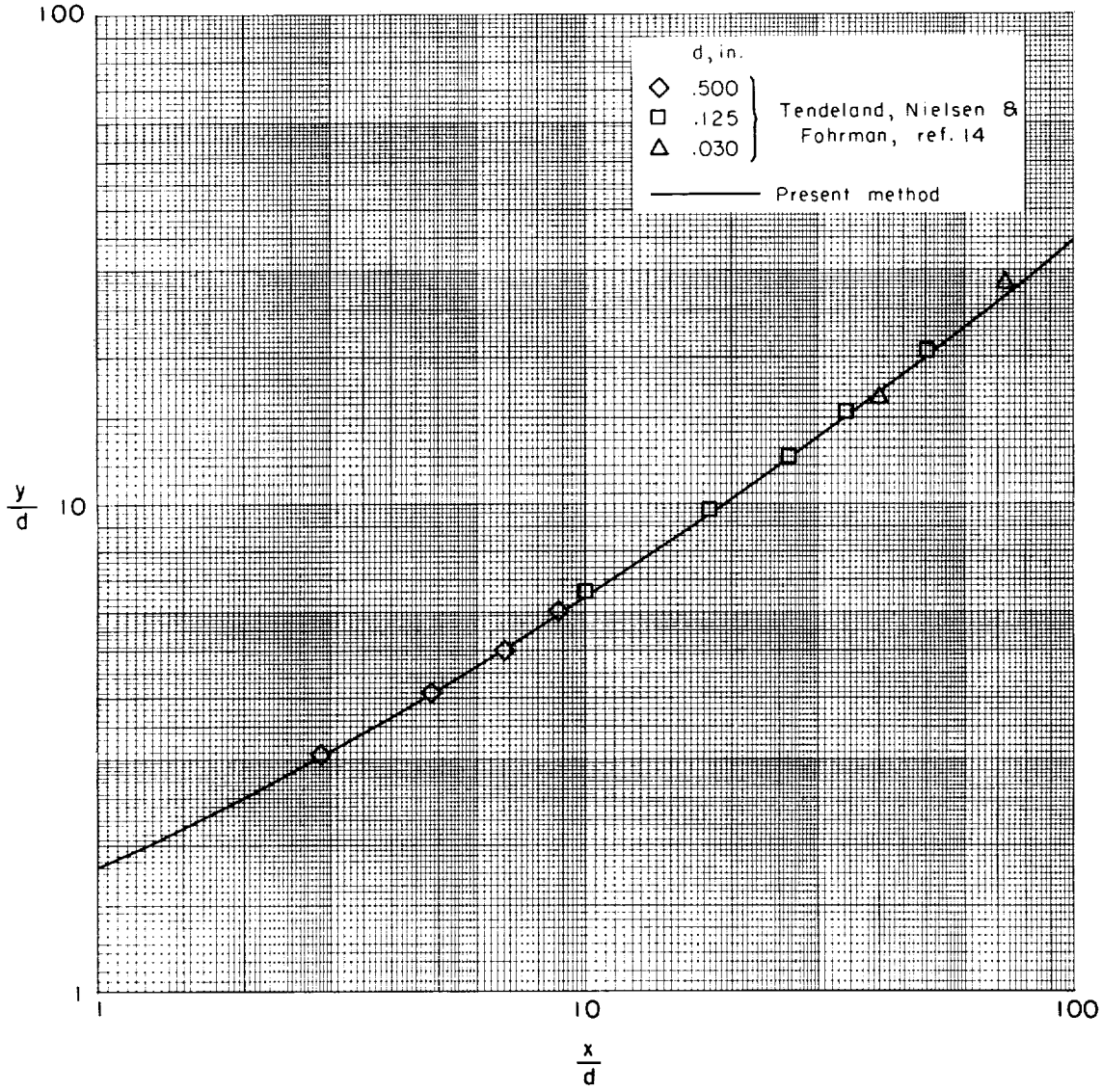

Figure 12.- Shock-wave shape for flat plate with cylindrical leading edge; $\gamma = 1.4$, $M_\infty = 4.7$.

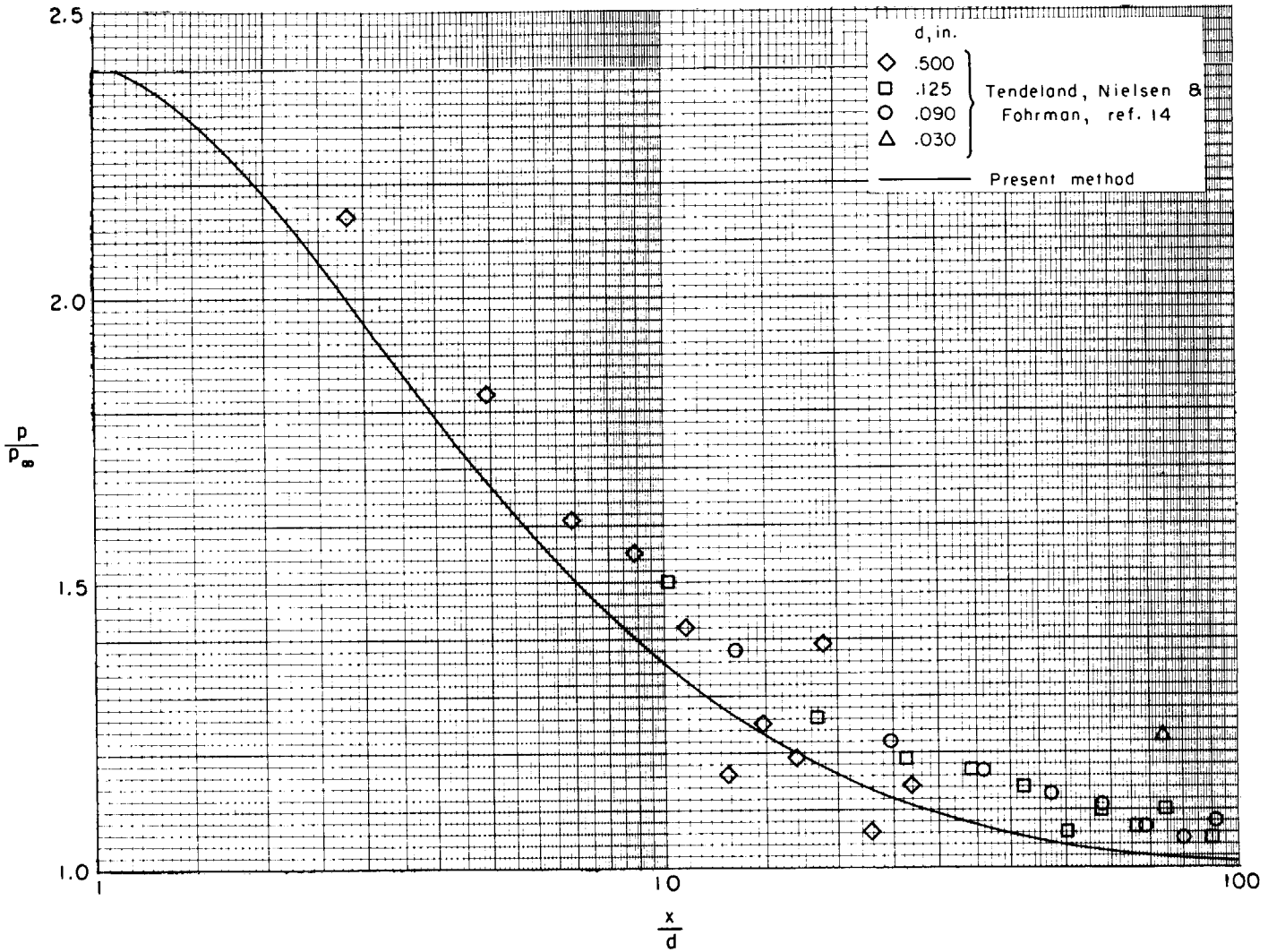

Figure 13.- Surface-pressure distribution on flat plate with cylindrical leading edge; $\gamma = 1.4$, $M_\infty = 4.7$.

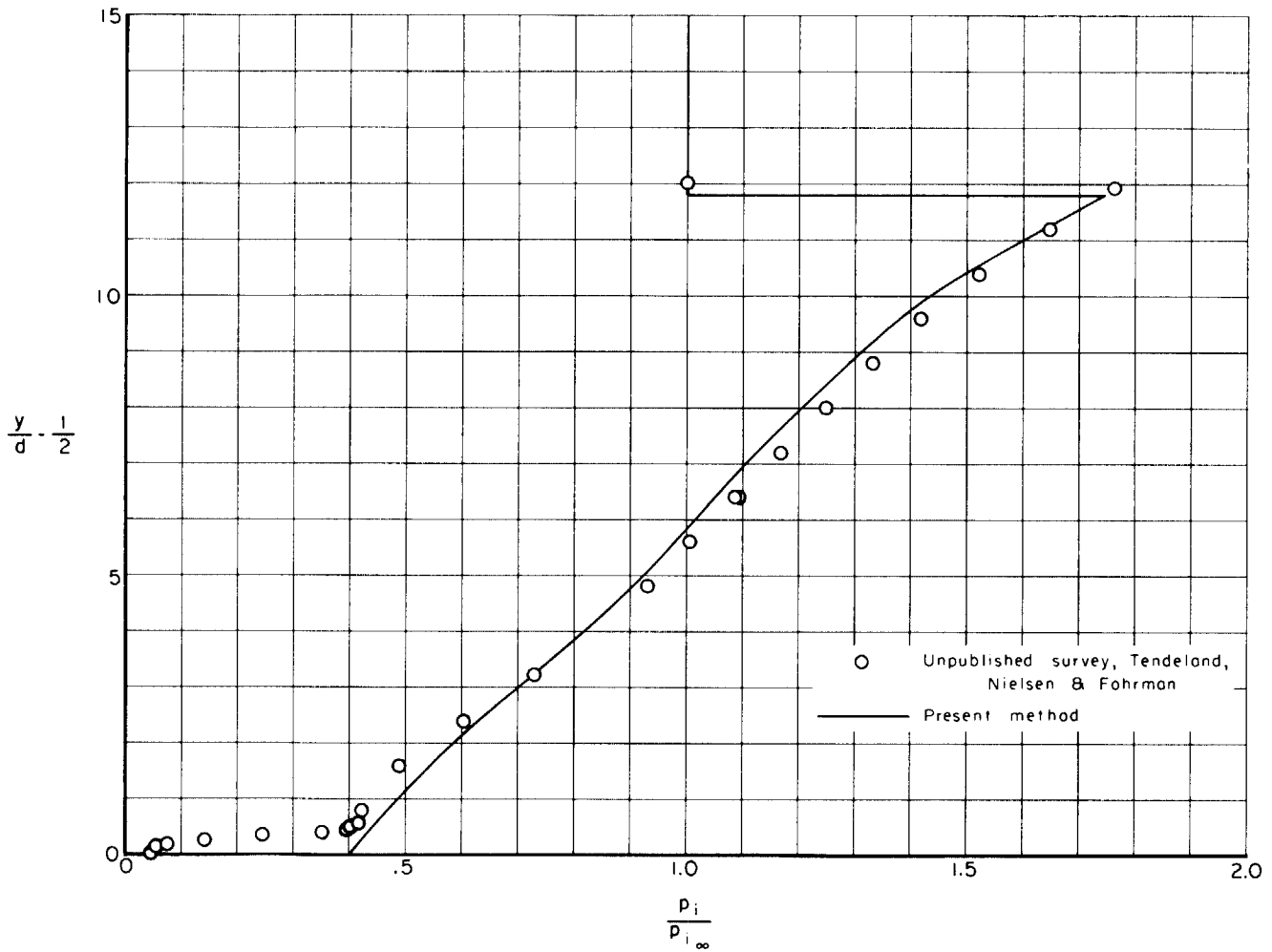

(a) x/d = 26.2

Figure 14.- Impact-pressure distribution between flat plate with cylindrical leading edge and shock wave; $\gamma = 1.4$, $M_\infty = 4.70$, d = 1/8 inch.

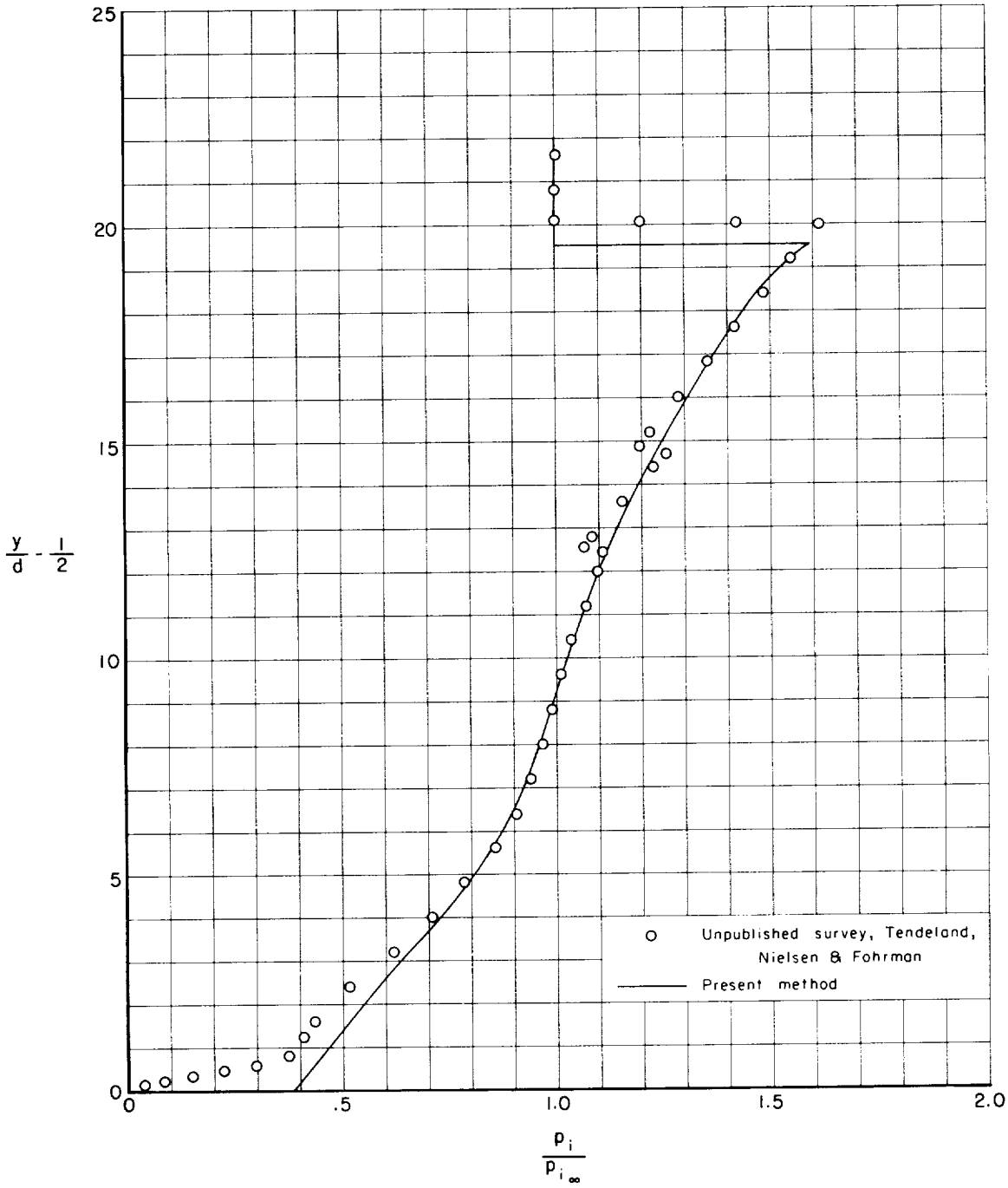

(b) x/d = 50.0

Figure 14.- Concluded.

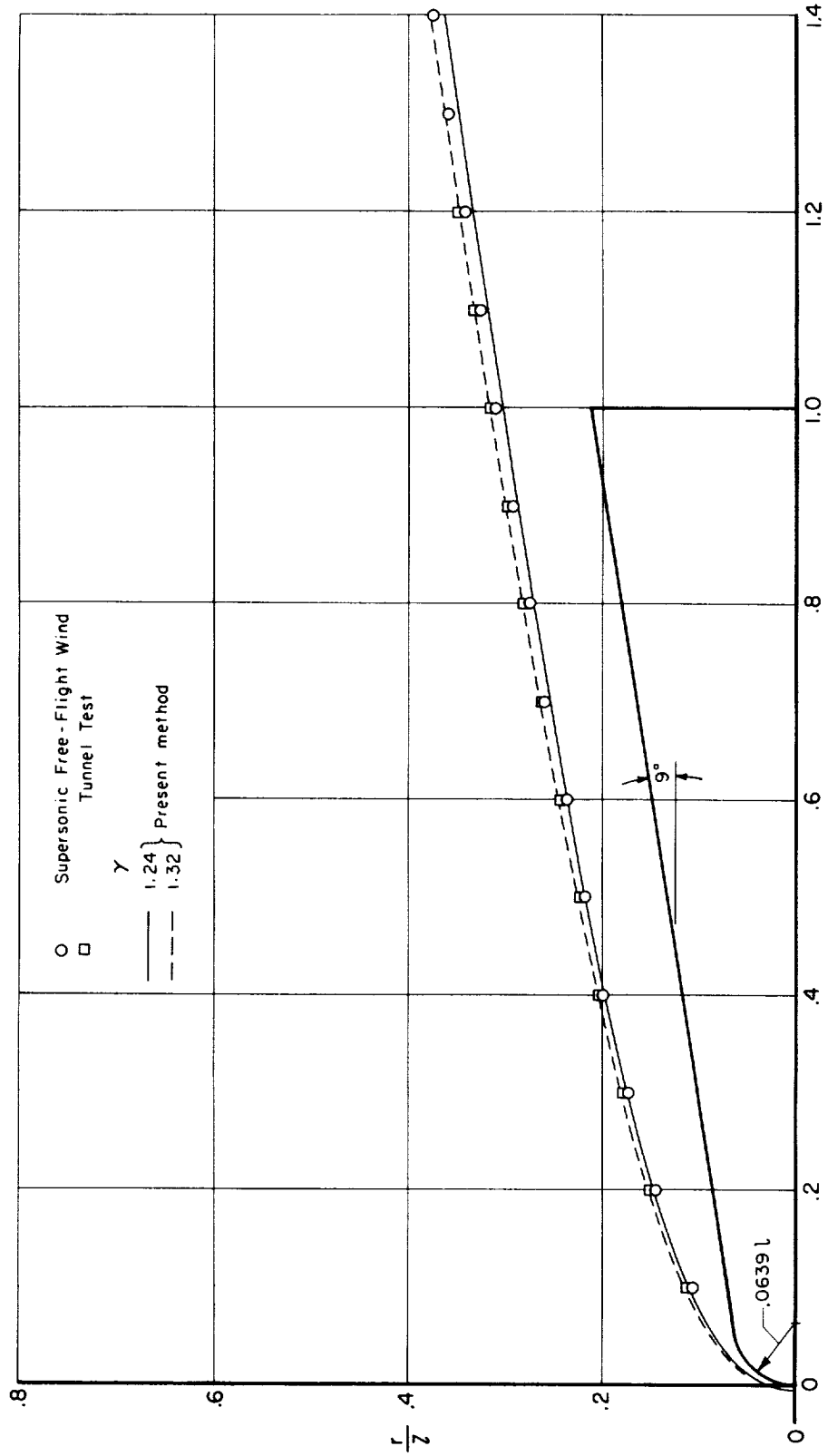

Figure 15.- Shock-wave shape for sphere-18° cone in air, $M_\infty = 17.8$, $T_\infty = 191.5^\circ$ R, $\rho_\infty = 0.9055 \times 10^{-3}$ lb sec^2/ft^4.